

1

2 **Single-molecule imaging of chromatin remodelers reveals**
3 **role of ATPase in promoting fast kinetics of target search**
4 **and dissociation from chromatin**

5

6 Jee Min Kim¹, Pat Visanpattanasin^{1,5}, Vivian Jou^{1,5}, Sheng Liu¹, Xiaona Tang¹, Qinsi
7 Zheng², Kai Yu Li¹, Jonathan Snedeker¹, Luke D. Lavis², Timothée Lionnet³, Carl Wu^{1,4,*}

8

9

10

11

12

13

14

15

16

17

18 ¹Department of Biology, Johns Hopkins University, Baltimore, MD 21218, USA

19 ²Janelia Research Campus, Howard Hughes Medical Institute, Ashburn, VA 20147,
20 USA

21 ³Institute of Systems Genetics, Langone Medical Center, New York University, New
22 York, NY 10016, USA

23 ⁴Department of Molecular Biology and Genetics, Johns Hopkins School of Medicine,
24 Baltimore, MD 21287, USA

25 ⁵These authors contributed equally

26 *Correspondence: wuc@jhu.edu

27

ABSTRACT

Conserved ATP-dependent chromatin remodelers establish and maintain genome-wide chromatin architectures of regulatory DNA during cellular lifespan, but the temporal interactions between remodelers and chromatin targets have been obscure. We performed live-cell single-molecule tracking for RSC, SWI/SNF, CHD1, ISW1, ISW2, and INO80 remodeling complexes in budding yeast and detected hyperkinetic behaviors for chromatin-bound molecules that frequently transition to the free state for all complexes. Chromatin-bound remodelers display notably higher diffusion than nucleosomal histones, and strikingly fast dissociation kinetics with 4-7 s mean residence times. These enhanced dynamics require ATP binding or hydrolysis by the catalytic ATPase, uncovering an additional function to its established role in nucleosome remodeling. Kinetic simulations show that multiple remodelers can repeatedly occupy the same promoter region on a timescale of minutes, implicating an unending ‘tug-of-war’ that controls a temporally shifting window of accessibility for the transcription initiation machinery.

KEYWORDS

ATP-dependent chromatin remodelers, single-molecule tracking, live-cell imaging, search and residence times, promoter region occupancy

INTRODUCTION

Eukaryotic chromatin is assembled in nucleosomes and higher order structures that compact the DNA for genome folding in the cell nucleus. Nucleosomes are actively organized at promoter and enhancer elements that are hypersensitive to nuclease digestion (Almer & Hörz, 1986; Heintzman et al., 2007; Wu, 1980). In the budding yeast *Saccharomyces cerevisiae*, gene promoters contain nucleosome-depleted regions (NDRs), approximately 150 base-pair stretches of DNA that are depleted of nucleosomes (Yuan et al., 2005). Non-canonical nucleosome conformations, often called ‘fragile nucleosomes’, and non-histone protein-DNA complexes, are also observed by limited MNase treatment and occupy a subset of NDRs (Floer et al., 2010; Kubik et al., 2015; Prajapati, Ocampo, & Clark, 2020). NDRs are flanked by well-

positioned +1 and -1 nucleosomes, with the +1 nucleosome overlapping the transcription start site (TSS) in yeast (Albert et al., 2007; Yuan et al., 2005). The +1 nucleosome also phases downstream nucleosome positions in regularly spaced locations which become progressively less well-positioned into the gene body (Lai & Pugh, 2017a; Mavrich et al., 2008). This arrangement of nucleosomes is important for the accurate engagement of transcription regulators and the transcription pre-initiation complex [PIC], as well as the progression of the transcription machinery after initiation.

ATP-dependent chromatin remodelers are key *trans*-acting factors in establishing and maintaining nucleosome organization around genes (Becker & Workman, 2013; Rando & Winston, 2012; Zhang et al., 2011). As specialized members of the superfamily 2 (SF2) translocases, chromatin remodeling enzymes share a highly conserved ATPase motor that utilizes DNA translocation as the fundamental mechanism to restructure DNA-histone contacts within nucleosomes. In addition to the core ATPase domain, chromatin remodelers harbor additional functional domains and accessory subunits, forming multiprotein complexes up to ~1 MDa in size that show substantial functional diversity. They are further classified into four sub-families based on sequence homology of the catalytic ATPase and possession of shared components, namely the SWI/SNF [Switch defective/sucrose non-fermenting], CHD [Chromodomain helicase DNA-binding], ISWI [Imitation switch], and INO80 [Inositol requiring 80] sub-families.

In vivo studies of remodelers in yeast revealed their distinct genome-wide specificities and functions in the multi-stage transcription process (Yen, Vinayachandran, Batta, Koerber, & Pugh, 2012). In this context, remodelers can be distinguished based on their *in vivo* specificities for nucleosome targets genome-wide. The first group of remodelers, RSC, SWI/SNF, INO80, and ISW2, mainly act at gene promoter regions to define the +1 and -1 nucleosome positions. RSC and SWI/SNF mobilize the +1 and -1 nucleosomes away from the NDR relative to the TSS to promote proper engagement of transcription initiation machinery (Ganguli, Chereji, Iben, Cole, & Clark, 2014; Klein-Brill, Joseph-Strauss, Appleboim, & Friedman, 2019; Kubik et al., 2018). Specifically, RSC assists NDR formation for the majority of yeast genes, and the consequence of conditional RSC

inactivation is a global loss of transcription (Brahma & Henikoff, 2019; Ganguli et al., 2014; Kubik et al., 2018; Yen et al., 2012). This has led to the concept of RSC (and SWI/SNF) as nucleosome ‘pushers,’ widening the NDR (Kubik et al., 2019). Antagonizing the pushing actions of RSC and SWI/SNF are INO80 and ISW2 (Klein-Brill et al., 2019; Kubik et al., 2019; Shimada et al., 2008; Yen et al., 2012). Both ISW2 and INO80 remodelers reposition the +1 and -1 nucleosomes towards the NDR *in vivo*, which is important for suppressing yeast cryptic transcription via noncanonical TSS usage (Klein-Brill et al., 2019; Kubik et al., 2019; Whitehouse, Rando, Delrow, & Tsukiyama, 2007). Furthermore, INO80 and ISW2 are implicated in DNA replication (Au, Rodriguez, Vincent, & Tsukiyama, 2011; Lee, Rodriguez, & Tsukiyama, 2015; Vincent, Kwong, & Tsukiyama, 2008) and INO80 in DNA damage repair (Morrison et al., 2004; Van Attikum, Fritsch, Hohn, & Gasser, 2004).

The second group of remodelers, CHD1 and ISW1, act primarily in the gene body where they maintain proper nucleosome spacing and density relative to the +1 nucleosome. Their actions are coupled to transcription elongation by interacting with the elongating polymerase to maintain nucleosome density and thus suppress cryptic initiation within the gene body (Cheung et al., 2008; Radman-Livaja et al., 2012; Smolle et al., 2012a). Remodelers with similar *in vivo* activities are functionally redundant as shown by stronger effects due to multiple deletions or depletions, compared to single deletion or depletion (Kubik et al., 2019; Ocampo, Chereji, Eriksson, & Clark, 2016). Furthermore, remodelers act competitively to fine-tune nucleosome positions around genes, leading to proper transcriptional regulation (Kubik et al., 2019; Ocampo et al., 2016; Ocampo, Chereji, Eriksson, & Clark, 2019; Parnell, Schlichter, Wilson, & Cairns, 2015). These results further highlight the current perspective that nucleosomes located around genes are highly dynamic rather than static, and that the concerted actions of multiple remodelers result in the striking steady-state nucleosome organization observed by genome-wide mapping experiments. However, despite this knowledge, a gap still lies in our understanding of their real-time dynamics and timescales of remodeler interactions on their chromatin targets.

Here we utilize single-molecule tracking (SMT) to directly observe and characterize the chromatin-binding kinetics of ATP-dependent chromatin remodelers in living cells (Lionnet & Wu, 2021). We investigated a comprehensive set of remodelers (RSC, SWI/SNF, CHD1, ISW1, ISW2, INO80) acting at gene promoter regions and gene bodies, allowing us to quantify and compare their *in vivo* dynamics. We show that remodelers have varying but substantial frequencies of chromatin binding, while exhibiting a common target search strategy of frequently engaging in highly transient (sub-second) chromatin interactions and stable residence times of only several seconds. We also discovered that the catalytic ATPase is responsible for enhancing their chromatin-associated diffusion and fast dissociation rates. By integrating the kinetic parameters measured for individual chromatin remodelers with values from genomic studies, we could simulate substantial temporal occupancies at yeast chromatin targets, leading to a tug-of-war model for the organization and dynamic positioning of the nucleosome landscape.

RESULTS

Chromatin remodelers exist in chromatin bound and free populations

We tagged the catalytic subunits of 6 major chromatin remodeling complexes, RSC, SWI/SNF, CHD1, ISW1 (ISW1a, and ISW1b), ISW2, and INO80 at the C-terminus with the self-labeling HaloTag by engineering the endogenous loci and expressed the fusion proteins as the sole source under natural promoter control. The fusion proteins were localized in the nucleus and did not display detectable cleavage of the tag by SDS-PAGE (Figure 1-figure supplement 1A, B). Furthermore, no phenotypes were observed for all strains containing tagged constructs (Figure 1-figure supplement 1C). We then investigated their endogenous, real-time dynamics as representative subunits of chromatin remodeling complexes in asynchronous, log-phase cells (Figure 1A).

In order to quantify a broad range of kinetic behaviors displayed by remodelers, two imaging regimes were applied. ‘Fast-tracking’ acquires 10 ms frame-rate movies to directly measure a range of single-molecule diffusivities from ‘slow’ (chromatin-bound) to ‘fast’ (chromatin-free) and determine fractional representation (Figure 1B, Video 1).

However, high laser power and extensive photobleaching precludes measurement of chromatin residence times. ‘Slow-tracking’ with a longer 250 ms frame-rate and lower laser power motion-blurs fast diffusing molecules to selectively visualize the chromatin-bound state and report dwell times (Figure 1C). Combining the two imaging regimes provides a holistic and quantitative view of a range of diffusive behaviors and kinetic subpopulations.

We applied two independent methods for visualization and quantification of fast-tracking datasets. First, we determined the diffusion coefficient D for trajectories ≥ 6 frames (i.e. ≥ 60 ms) based on their mean squared displacements (MSD), and present frequency histograms based on the $\log(D)$ values of each trajectory. The histograms were initially fit to two Gaussian distributions, approximating slow and fast populations (Figure 1-figure supplement 4, Figure 1-source data 1). For more robust quantification, we applied Spot-On analytics, which uses kinetic modeling based on distribution of displacements for trajectories lasting ≥ 3 frames (Hansen et al., 2018) (Figure 1-figure supplement 2A,B). Hereafter, we refer to diffusive values derived from Spot-On in the text. As previously reported for biological controls, H2B histone (Halo-H2B) and free HaloTag (Halo-NLS, nuclear localization signal), exhibit two distinct, well-separated diffusion states representing chromatin-bound and chromatin-free molecules (Ranjan et al., 2020). We found that the majority of H2B molecules ($79.4 \pm 1.9\%$) are slow-moving with average D of $0.026 \mu\text{m}^2\text{s}^{-1}$ (Figure 1-figure supplement 2A) consistent with incorporation into chromatin, whereas most of the chromatin-free Halo-NLS molecules show greatly increased diffusivity ($D \sim 5 \mu\text{m}^2\text{s}^{-1}$) (Ranjan et al., 2020).

Compared to H2B, chromatin remodelers exhibit a slow D_{bound} fraction (average 0.036 ± 0.007 to $0.067 \pm 0.004 \mu\text{m}^2\text{s}^{-1}$) as would be expected for molecules associated with largely immobile chromatin (Figure 1-figure supplement 2A). However, as discussed later, the D_{bound} values are ~ 2 -fold higher than H2B. Furthermore, we also observed a separable chromatin-free fraction whose D_{free} values (0.464 ± 0.043 to $1.014 \pm 0.024 \mu\text{m}^2\text{s}^{-1}$) are ~ 10 -fold higher, but distinctly lower than the D_{free} for Halo-NLS, indicating that our imaging regime captures essentially the full range of potential diffusive

183 behaviors for this family. In addition, the D_{free} values show an inverse correlation with
184 the estimated total molecular
185

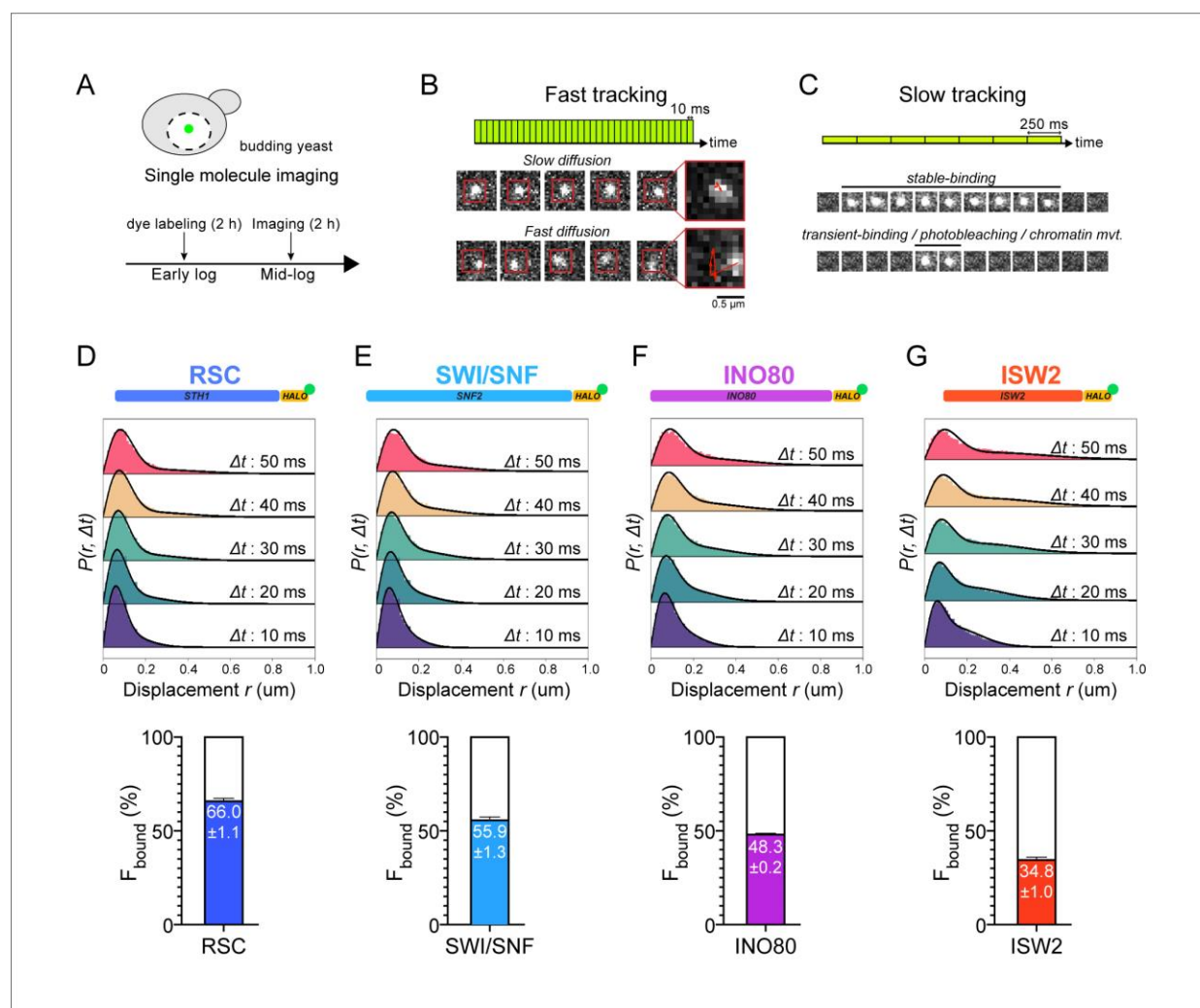


Figure 1. Chromatin-binding and chromatin-free fractions of RSC, SWI/SNF, INO80, and ISW2. (A) Experimental scheme. (B) Fast-tracking imaging regime uses short exposures (10 ms) at high laser power to distinguish slow (chromatin-bound) and fast (chromatin-free) diffusing populations. (C) Slow-tracking regime directly observes the dwell times of chromatin-bound molecules using 250 ms exposures at low laser power. (D-G) (Top) Raw displacement histograms over the first 5 time frames (Δt : 10, 20, 30, 40, 50 ms). A two-state kinetic model was used for fitting the CDF [black lines] in Spot-On. (Bottom) Spot-On kinetic modeling results based on displacement distribution histograms for Sth1-Halo (D), Snf2-Halo (E), Ino80-Halo (F), and Isw2-Halo (G). Solid colored bar with indicated value represents % chromatin-bound molecules; open bar represents % chromatin-free. Error bars are standard deviations from 2 [or 3 for ISW2] biological replicates.

Figure supplement 1. Cell growth, integrity, and localization of HaloTagged remodeler subunits.

Figure supplement 2. Spot-On kinetic modeling analysis.

Figure supplement 3. Yeast culture during imaging and laser illumination do not have obvious effects on remodeler diffusion.

Figure supplement 4. Log₁₀D histograms for six remodelers and Gaussian fitting.

Source data 1. MSD-based kinetic analysis.

Source data 2. Original gel images for Figure supplement 1A.

weights of chromatin remodeling complexes, consistent with expectations that the tagged catalytic subunits are associated within larger complexes (Figure 1-figure supplement 1D). We note that additional subpopulations, including variant or modified complexes, could be included within our two diffusive populations distinguishable by SMT.

We next assessed how the fractions of chromatin-bound and chromatin-free molecules vary among subgroups of chromatin remodeling enzymes. RSC and SWI/SNF mobilize +1 and -1 nucleosomes to increase promoter accessibility, while INO80 and ISW2 mobilize them to reduce accessibility (Hartley & Madhani, 2009; Kubik et al., 2019). We found that the majority of both RSC and SWI/SNF molecules are associated with chromatin (RSC: $66.0 \pm 1.1\%$; SWI/SNF: $55.9 \pm 1.3\%$) (Figure 1D,E). INO80 and ISW2 exhibit F_{bound} values of $48.3 \pm 0.2\%$ and $34.8 \pm 1.0\%$, respectively (Figure 1F,G). Overall, these NDR-acting remodelers display a broad range of chromatin-binding fractions (inclusive of stable and transient binding), with RSC showing the highest overall chromatin binding.

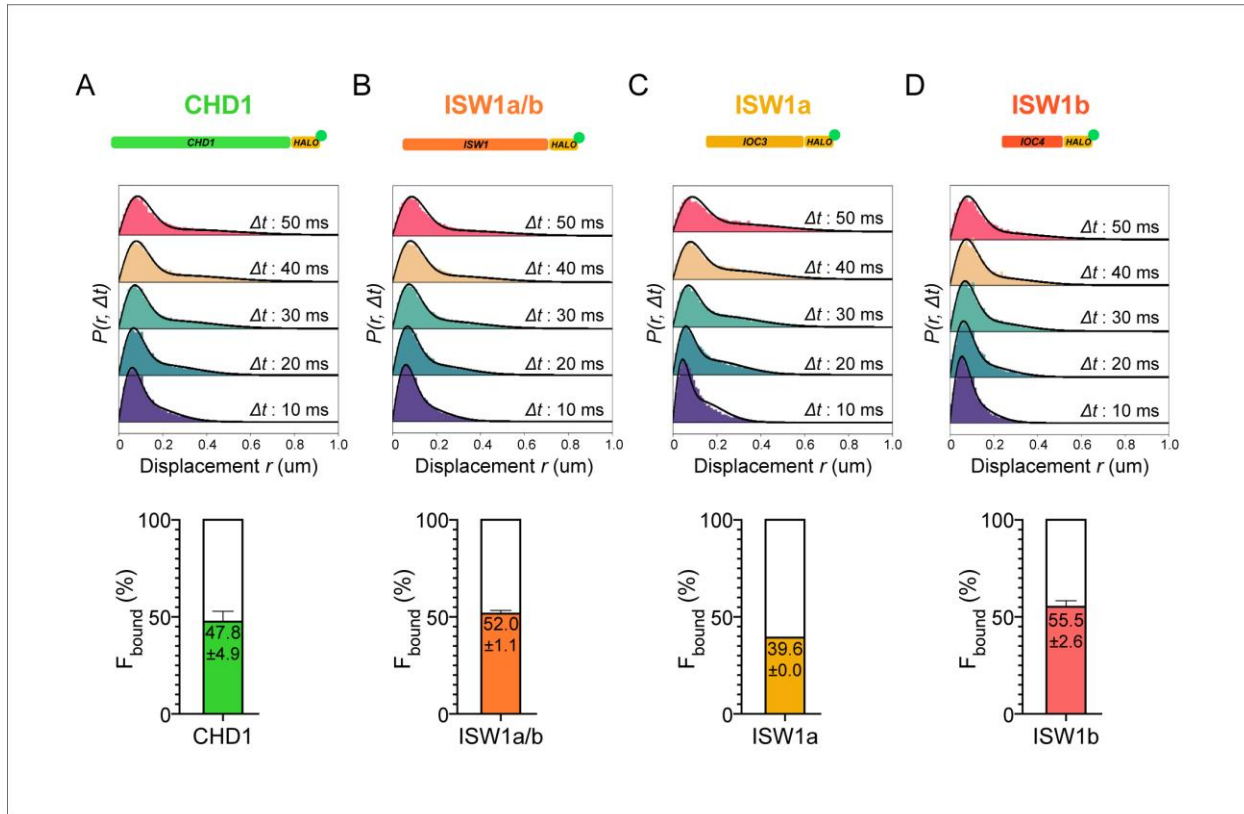


Figure 2 Chromatin-binding and chromatin-free populations of CHD1 and ISW1. (A-B) Spot-On analysis as described in Figure 1 for the catalytic subunits Chd1-Halo (A) and Isw1-Halo (B). (C-D) Spot-On analysis of the accessory subunits of ISW1a and ISW1b complexes: loc3-Halo (C) and loc4-Halo (D).

CHD1 and ISW1 act primarily on nucleosomes located in the gene body (Kubik et al., 2019; Ocampo et al., 2016). The two remodelers show comparable F_{bound} values (CHD1: $47.8 \pm 4.9\%$; ISW1a/b: $52.0 \pm 1.1\%$) (Figure 2A,B). However, the catalytic subunit Isw1 is shared by two distinct chromatin remodeling complexes called ISW1a and ISW1b (Vary et al., 2003), in addition to potentially un-complexed Isw1 catalytic subunit (Tsukiyama, Palmer, Landel, Shiloach, & Wu, 1999). The ISW1a complex localizes near the transcription start and end of genes, whereas the ISW1b complex occupies more mid-coding regions (Morillon et al., 2003; Smolle et al., 2012b; Yen et al., 2012). Since Isw1 catalytic subunit dynamics represent a composite of the two remodeling complexes, we also tagged loc3 and loc4 accessory subunits unique to ISW1a and ISW1b complexes, respectively. The gene-body acting ISW1b (loc4-Halo)

complex exhibits higher F_{bound} compared to ISW1a (loc3-Halo) complex (ISW1b: $55.5 \pm 2.6\%$; ISW1a: $39.6 \pm 0.0\%$) (Figure 2C,D).

Chromatin remodelers frequently transition between bound and free states

Unlike the two well-separated Gaussian distributions for H2B histones and HaloTag protein (Figure 3A), the Log(D) histograms of all imaged chromatin remodelers display less distinct bound and free populations, with a noticeable fraction showing an intermediate range of diffusion coefficients (Figure 1-figure supplement 4). This population could either represent remodeler complexes transitioning between chromatin-bound and chromatin-free states, or chromatin-free molecules of intermediate diffusivity due to association with additional factors or confined inside a subnuclear compartment (Hansen, Amitai, Cattoglio, Tjian, & Darzacq, 2020; Izeddin et al., 2014; McSwiggen et al., 2018; Strom et al., 2017).

To distinguish between these possibilities, we analyzed single-particle trajectories using vbSPT, a variational Bayesian Hidden Markov Model (HMM) algorithm, which models state kinetics and assigns diffusive states to each displacement (Persson, Lindén, Unoson, & Elf, 2013). We classified every displacement as either State 1 ('bound') or State 2 ('free') (Figure 3-source data 1), and sub-classified all trajectories as bound, free, or transitioning (Figure 3B). The median bound and free displacement lengths between transitioning and non-transitioning trajectories are highly similar or identical for each remodeler, validating the vbSPT state assignments and essentially excluding a dominant intermediate diffusive state (Figure 3-figure supplement 1A-C). Notably, the log D histograms of transitioning populations show enrichment for intermediate D values.

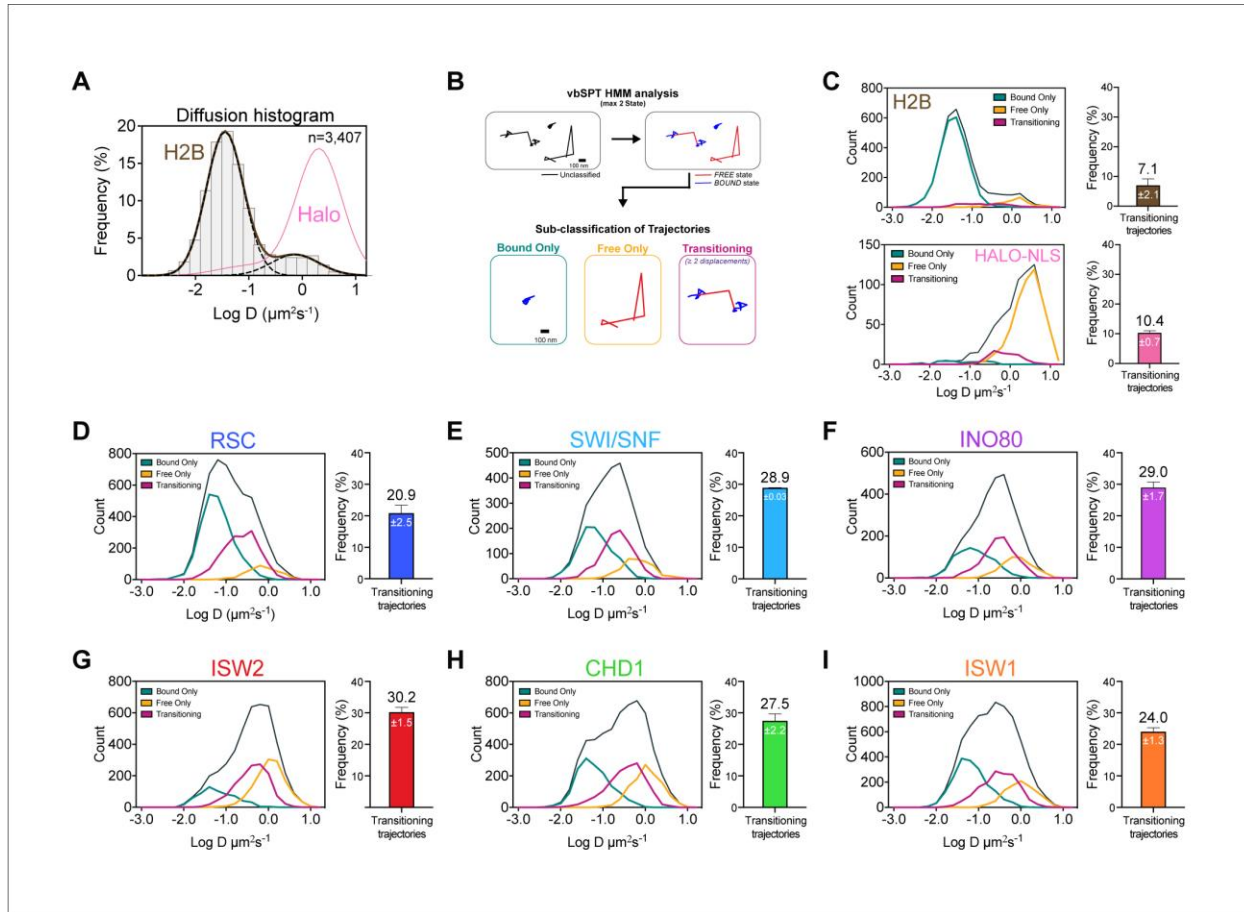


Figure 3. Remodelers undergo frequent transitions between bound and free states.

(A) Halo-H2B (brown) and Halo-NLS (pink) molecules display well-separated peaks in diffusion coefficient histograms. (B) An overview of displacement-based HMM classification (vbSPT) to identify transitioning trajectories. After classifying each displacement as either in bound or free state, each trajectory is sub-classified as 'bound only', 'free only', or 'transitioning'. (C-I) Left: Overlay of raw histograms of \log_{10} diffusion coefficients for 'Bound only' (turquoise), 'Free only' (yellow), 'Transitioning' (purple), and total trajectories (thin black). Right: Quantification (%) of transitioning trajectories in the diffusion coefficient histogram, where errors represent standard deviation between 2 [or 3 for ISW2] biological replicates. (C) Transitioning trajectories for Halo-H2B (top) and Halo-NLS (bottom). (D-I) Transitioning trajectories for remodelers: Sth1-Halo (D), Snf2-Halo (E), Ino80-Halo (F), and Isw2-Halo (G), Chd1-Halo (H), and Isw1-Halo (I).

Figure supplement 1. Validation of two diffusive states classified by vbSPT, and quantification of transitioning frequencies.

Source data 1. vbSPT analysis.

It is striking that the population of transitioning trajectories is more prominent for remodelers (from $20.9 \pm 2.5\%$ to $30.2 \pm 1.5\%$) compared to free HaloTag ($10.4 \pm 0.7\%$) and H2B histone ($7.1 \pm 2.1\%$), (Figure 3C-I, Figure 3-figure supplement 1D-E). We observed comparable frequencies for remodeler dissociation (bound to free transition:

45.3 \pm 1.3 to 50.24 \pm 0.01 %) and association (free to bound: 49.76 \pm 0.01 to 54.7 \pm 1.3%), indicating that there is little bias in the direction of state transitions (Figure 3-figure supplement 1F). Furthermore, the frequent detection of state transitions over short trajectory lifetimes suggests that the duration of each state is short-lived. We concluded that transient but frequent chromatin interactions are characteristic of the six remodeling complexes.

All remodelers have remarkably short *in vivo* residence times of 4-7 s

The chromatin-bound remodeler population measured by fast tracking consists of both transiently and stably bound molecules. We acquired long-exposure movies [250 ms/frame] under slow tracking (Chen et al., 2014) to generate survival curves revealing the apparent dissociation of chromatin-bound molecules as a function of time (Figure 1C). Particle dissociation can be due to molecules truly disengaging from chromatin, or to fluorophore photobleaching and chromatin movements out of focus, which can be corrected using the survival curve of H2B histone as a standard (Hansen, Pustova, Cattoglio, Tjian, & Darzacq, 2017). The remodeler survival plots fit well to a double exponential decay model (Figure 4-figure supplement 1A-F,H), from which the average lifetimes (τ_{sb} , τ_{tb}) and fractions (f_{sb} , f_{tb}) of stable-binding and transient-binding species were extracted (Figure 4). All τ values presented in the text and figures are corrected based on H2B decay kinetics.

The stable-binding subpopulations (f_{sb}) of RSC (27 \pm 2%) and SWI/SNF (24 \pm 6%) display strikingly short lifetimes (RSC: 5.0 \pm 0.7 s; SWI/SNF 4.4 \pm 1.2 s) (Figure 4A,B), consistent with a previous measurement for the Rsc2 subunit of RSC (Mehta et al., 2018). Similarly, INO80 and ISW2 exhibit stable-binding fractions (f_{sb} 20 \pm 3% and 13 \pm 3%, respectively) and similarly short residence times (τ_{sb} 3.7 \pm 0.8 s and 4.9 \pm 2.2 s, respectively) (Figure 4C,D). Hence, all NDR-acting remodelers bind stably for less than 5 s in live yeast, whereas transient-binding populations are more short-lived by almost an order of magnitude (Figure 4-source data 1).

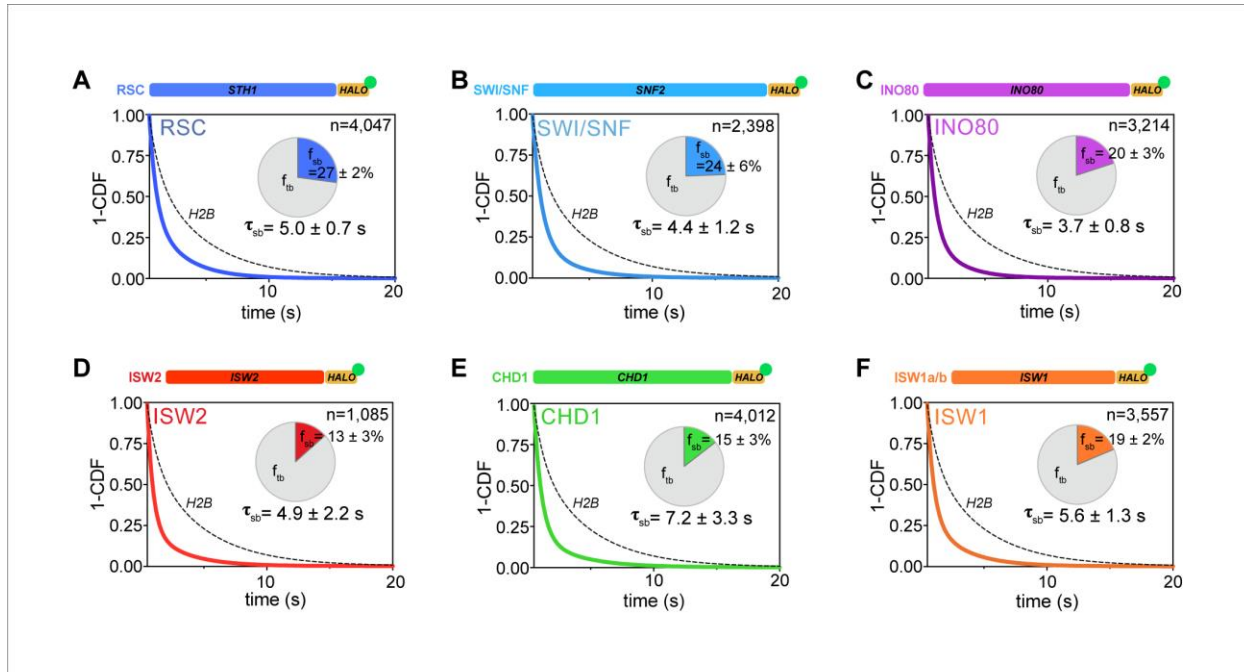


Figure 4. All remodelers have short-lived stable-binding residence times of 4-7 s.

(A-F) Fitted double exponential decay curves from 1-CDF plots of observed dwell times from individual binding events (n) imaged by slow-tracking, for Sth1-Halo (A) Snf2-Halo (B), Ino80-Halo (C), and Isw2-Halo (D), Chd1-Halo (E), and Isw1-Halo (F). Solid colored and dashed black fitted curves for indicated remodelers and H2B, respectively. Pie charts show the percentage (f_{sb}) and average residence time (τ_{sb}) of the stable binding population after photobleaching correction. Errors represent bootstrap resampling errors after resampling 100 times (sb: stable-binding; tb: transient-binding).

Figure supplement 1. Survival plots [1-CDF] of dwell times showing 1- vs 2-component exponential decay fits.

Source data 1. Kinetic parameters determined by slow-tracking.

For gene body-acting remodelers, CHD1 and ISW1 complexes exhibit stable-binding fractions (f_{sb} 15 ± 3% and 19 ± 2%, respectively) and short dwell times (τ_{sb} 7.2 ± 3.3 s and 5.6 ± 1.3 s, respectively) (Figure 4E,F). Interestingly, ISW1b shows 2.5-fold higher residence times compared to ISW1a (τ_{sb} 5.9 ± 2.5 s and 2.2 ± 1.0 s, respectively) with comparable stable-binding fractions (Figure 4-figure supplement 1G). These remodelers also exhibit very short transient-binding residence times (τ_{tb} < 0.65 s). Hence, the majority of chromatin binding events by remodelers is transient, and stable binding, on the order of several seconds, is notably short-lived.

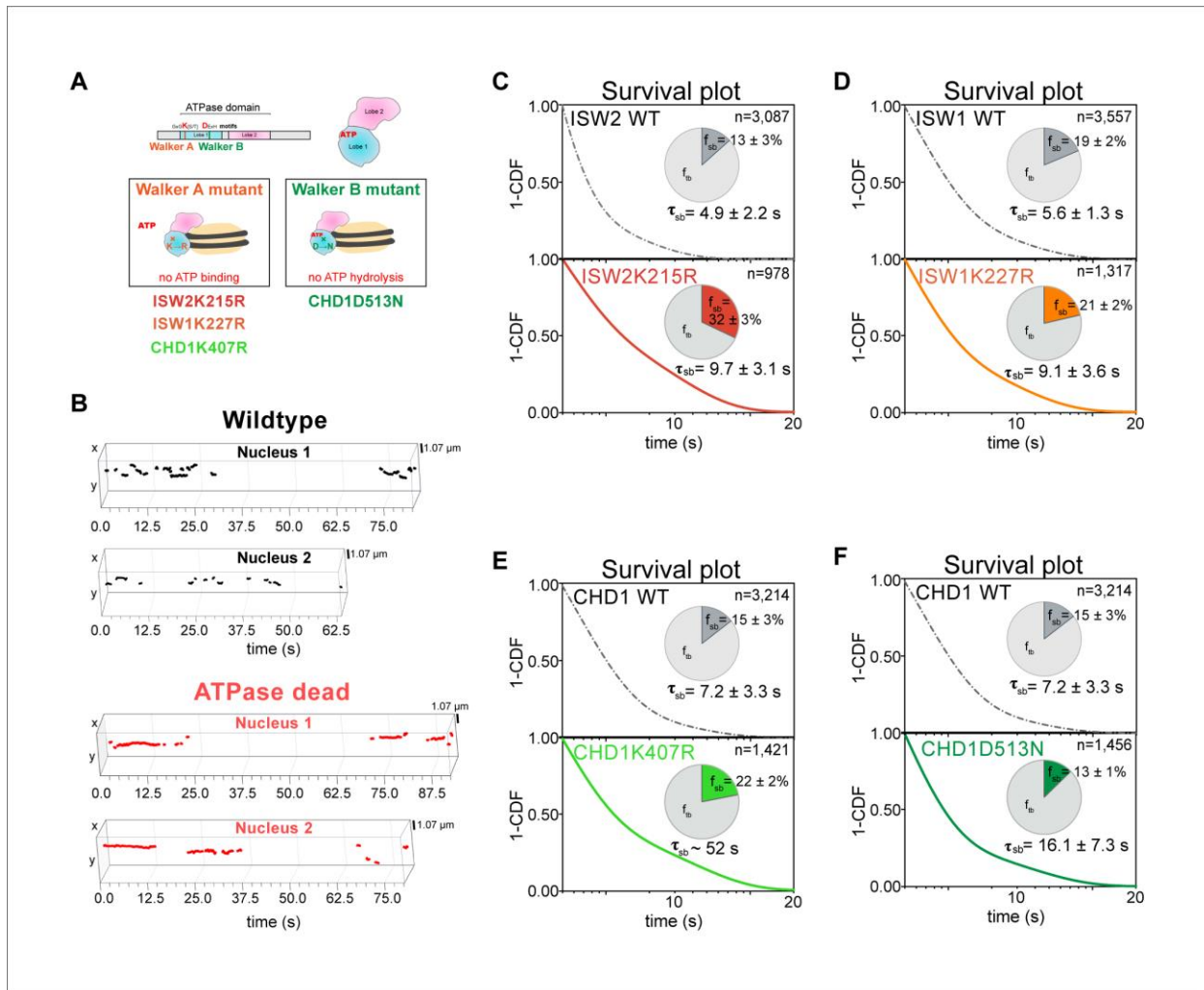


Figure 5. ATP hydrolysis is responsible for rapid chromatin dissociation.

(A) Bar diagram and cartoons for remodelers mutated in the 'Walker A' and 'Walker B' motifs, respectively. (B) Representative 3D plots of trajectories imaged by slow-tracking for wildtype (Chd1-Halo, black) and ATPase-dead mutant (Chd1K407R-Halo, red). Each plot shows all trajectories (≥ 3 frames) from single nucleus where lines represent apparent durations of chromatin-binding events. (C-F) 1-CDF plot, pie chart, and residence times of wildtype (top) and ATPase-dead mutants (bottom) for Isw2 (C), Isw1 (D), and Chd1 (E,F).

Figure supplement 1. Expression levels and 1-CDF plots for wildtype and mutant ATPase-dead Isw2D312N.

Source data 1. Slow-tracking for ATPase-dead mutants.

Source data 2. Original gel images for Figure supplement 1A.

ATPase activity is coupled to fast dissociation rates

To examine whether the measured dissociation kinetics are intrinsic to chromatin remodeling complexes or functionally related to their ATP-dependent remodeling activities, we made strains harboring a point mutation in the ATPase domains of Isw2, Isw1, and Chd1; these mutations have previously been shown to abolish their ATPase

activities (Isw2K215R, Isw1K227R, Chd1K407R, and Chd1D513N) (Figure 5A) (Fitzgerald et al., 2004; Gelbart, Rechsteiner, Timothy, Tsukiyama, & Richmond, 2001; Hauk, McKnight, Nodelman, & Bowman, 2010; Tsukiyama et al., 1999). We then acquired slow-tracking movies to compare the dwell times of mutant to those of wildtype remodeling enzymes (Figure 5B)

We found that the stable-binding average residence time increased by ~2-fold (from 4.9 ± 2.2 to 9.7 ± 3.1 s) for the Isw2K215R mutant (Figure 5C). Similarly, we observed increased residence time (from 5.6 ± 1.3 to 9.1 ± 3.6 s) for the Isw1K227R (Figure 5D). The two ATPase-dead Chd1 mutants both showed increased stable-binding residence times (Chd1K407R from 7.2 ± 3.3 to ~52 s; Chd1D513N from 7.2 ± 3.3 to 16.1 ± 7.3 s) (Figure 5E,F). Interestingly, the tail of the Chd1K407R survival curve approaches that of H2B, which indicates its longevity, but precludes precise determination of dwell time (Figure 5-figure supplement 1B). All four mutants (Figure 5-source data 1) exhibit little to no changes in the transient-binding residence times compared to wildtype. In all, our results indicate that after chromatin association, the mutant ATPases exhibit slower dissociation rate (the reciprocal of residence time), consistent with previous genome-wide ChIP and biochemical studies (Fitzgerald et al., 2004; Gelbart et al., 2001).

ATP binding enhances chromatin-bound mobility of remodelers

Chromatin imaged by several distinct methods in living cells displays heterogeneous mobility, which is dependent on its compaction state, subnuclear localization, and ATP-dependent processes (Gasser, 2002; Gu et al., 2018; Marshall et al., 1997; Soutoglou & Misteli, 2007). Remodelers may undergo 1D translocation on DNA (Sirinakis et al., 2011), and alter either local chromatin movement (Basu et al., 2020; Neumann et al., 2012) or higher-order chromatin structure (Lusser, Urwin, & Kadonaga, 2005; Maier, Chioda, Rhodes, & Becker, 2008) in an ATP-dependent fashion. We assessed the diffusive behavior of the chromatin-bound fraction of remodelers relative to the average dynamics of incorporated Halo-H2B histone. H2B not only reflects the motions of bulk chromatin but also provides an internal reference standard for nuclear movements and instrumental drift. From each trajectory classified as bound by vbSPT, the apparent D

value and the R_c [radius of confinement] were calculated to characterize its diffusivity and the confined domain encompassing the observed trajectory, respectively (Lerner et al., 2020). Importantly, chromatin-bound remodelers exhibit ~2-fold higher mobility than H2B histone, as revealed by the average MSD plot and the distribution of individual D values of each trajectory under fast-tracking (Figure 6A,B). The mean R_c values are also substantially higher for remodelers compared to the global mean measured for H2B (Figure 6-figure supplement 1A). This is further supported by the higher apparent D values to varying degrees [2- to 4-fold] of stably-bound remodelers measured by slow-tracking (Figure 6C). Such greater mobility of chromatin-bound remodelers may be due to the combined effects of remodeler diffusion on chromatin and movement of the chromatin fiber caused by remodeling activity, or alternatively, may reflect the intrinsic dynamics of genomic loci being targeted.

To distinguish between these two alternatives, we measured the chromatin-associated mobility of the four aforementioned ATPase-dead mutants. Three mutants Isw2K215R, Isw1K227R, Chd1K407R harboring substitutions in the catalytic ATPase Walker A motif responsible for ATP binding display strikingly lower diffusivity as revealed by the average MSD plot of stably bound molecules, which approaches or substantially overlaps the global H2B curve (Figure 6D-F). This is supported by the violin plots of individual D values for stably bound trajectories (Figure 6G). Surprisingly, Chd1D513N bearing a substitution in the Walker B motif of Chd1 shows no substantial changes in the average MSD curve and apparent D values for stably bound trajectories compared to wildtype as measured by slow-tracking (Figure 6F,H). To rule out Chd1-specific effects, we also made a strain harboring the corresponding D-to-N substitution in ISW2 (Isw2D312N), and found no substantial changes in the average MSD curve and apparent D values compared to wildtype (Figure 6D,H). As expected for a mutation in the catalytic ATPase, the Isw2D312N mutant exhibits an approximately two-fold increase in its residence time compared to wildtype (Figure 5-figure supplement 1C). Because the Walker B motif is important for ATP hydrolysis (via coordinating Mg^{2+} ion and a water molecule), but not for ATP binding (Singleton, Dillingham, & Wigley, 2007; Walker, Saraste, Runswick, & Gay, 1982) (Figure 5A), this result suggests that the ATP-

bound state may be adequate to induce enhanced diffusion on chromatin as part of the mechanism of target search by remodeling enzymes.

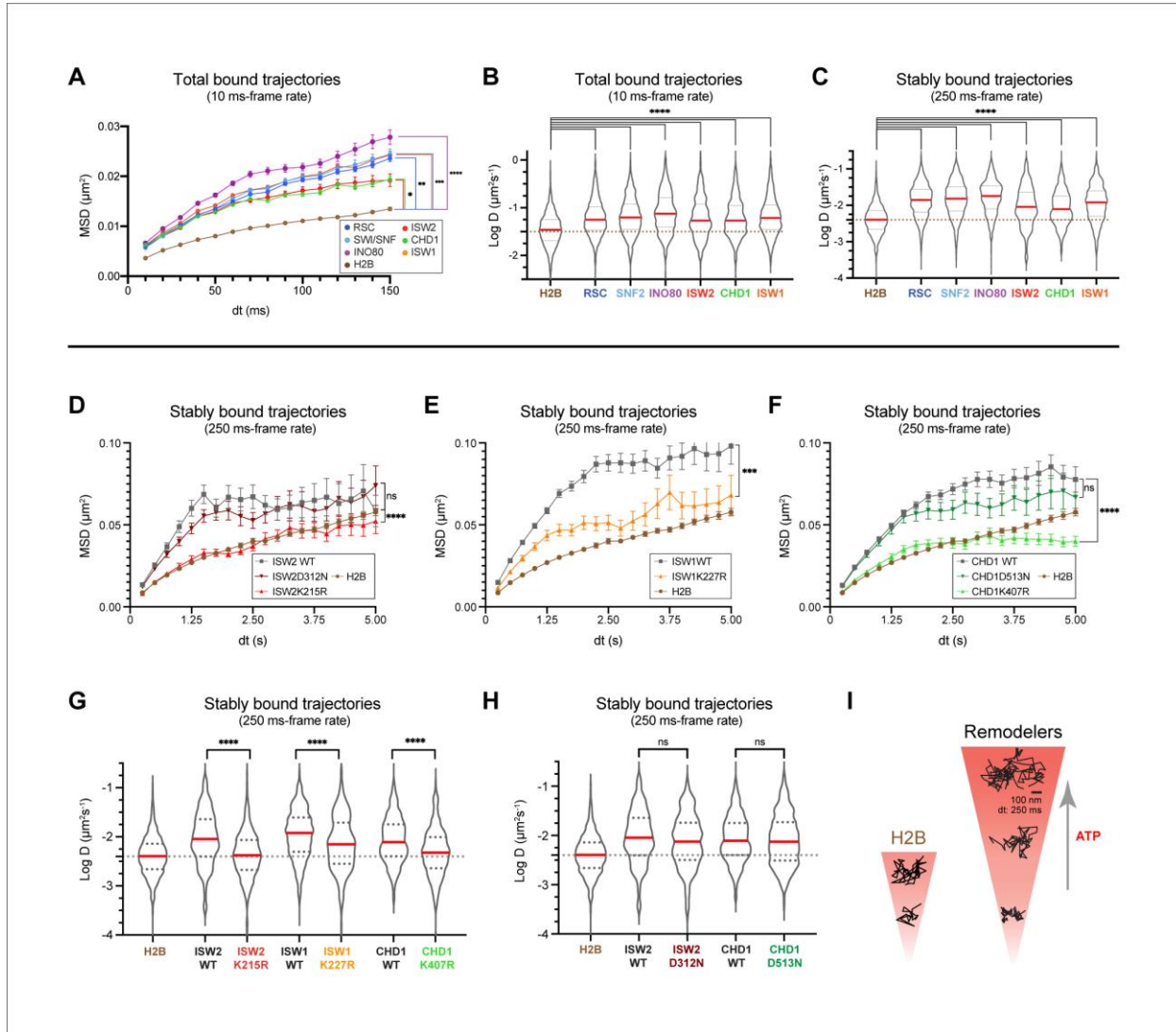


Figure 6. ATP utilization is responsible for enhanced mobility of chromatin-bound remodeler.

(A-B) Average MSD plot (A) and violin plot (B), of individual D values for 'bound only' trajectories imaged by fast-tracking, shown for six remodelers and H2B histone. (C) Violin plot showing distribution of individual D values imaged by slow-tracking for six remodelers and H2B histone. For A-C, each wildtype remodeler is compared to H2B by the ordinary one-way ANOVA test (**** $p < 0.0001$, *** $p < 0.001$, ** $p < 0.01$, * $p < 0.05$). (D-H) MSD plot (D-F) and violin plot (G,H) of individual D values for trajectories imaged by slow-tracking for wildtype, ATPase-dead mutant, and H2B. For violin plots, thick red and dotted gray lines represent the median and two quartiles, respectively. For D-H, mutants are compared to wildtype by the unpaired t test (**** $p < 0.0001$, *** $p < 0.001$, ns: not significant). (I) Representative trajectories imaged by slow-tracking for H2B and remodelers. H2B displays low mobility, whereas remodelers display higher chromatin-associated diffusivity that is enhanced by ATP utilization.

Figure supplement 1. Chromatin-bound remodelers display higher radius of confinement (R_c) values than H2B.

Source data 1. Number of molecules (N), statistical tests, and source data for Figure 6.

Promoter-enriched remodelers have robust chromatin occupancies

Chromatin remodelers are key regulators of the +1 nucleosome position genome-wide, whose accurate location is crucial for the PIC (pre-initiation complex) formation and TSS fidelity (Lai & Pugh, 2017b; Zhang et al., 2011). RSC and SWI/SNF mobilize the +1 nucleosome away from the NDR, opposed by INO80 and ISW2 activities, which slide the +1 nucleosome towards the NDR. As a quantitative indicator of nucleosome engagement, we determined the occupancies of the four remodelers, i.e. the percent average occupancy at a chromatin target by each remodeler over a given time period. To calculate temporal occupancy, we utilized the measured overall chromatin-binding fraction [F_{sb}] and the temporal parameters for stable [T_{sb} , f_{sb}] and transient [T_{tb} , f_{tb}] chromatin-binding (Figure 7A). Here, we assume that stable binding, which is almost an order of magnitude longer than transient binding, represents binding at 'specific' target sites within promoter regions including -1, +1 nucleosomes and the intervening NDR, while transient binding represents non-specific chromatin interactions (Ball et al., 2016).

The fraction of stable-binding depends on both the number of molecules per nucleus ($N_{molecules}$) and number of the target sites in the genome ($N_{targets}$) (Chen et al., 2014). We rely on published values for $N_{molecules}$ compiled from a meta-analysis of twenty-one proteomic studies for the best available quantitative estimate of remodeler abundance in *S. cerevisiae* (Ho, Baryshnikova, & Brown, 2018), with the assumption that our sole source HaloTag fusions under natural promoter control are similar in abundance to the untagged proteins. As regards the number of chromatin targets ($N_{targets}$), many studies have investigated the genome-wide specificities of chromatin remodelers using multiple approaches including ChIP-Seq (Cutler, Lee, & Tsukiyama, 2018; Floer et al., 2010; Shimada et al., 2008; Spain et al., 2014), MNase-ChIP (Yen et al., 2012), ChIP-exo (Rossi et al., 2021), Native-ChIP-Seq (Ramachandran, Zentner, & Henikoff, 2015; Zentner, Tsukiyama, & Henikoff, 2013), CUT&RUN (Brahma & Henikoff, 2019), and ChEC-seq (Kubik et al., 2019). For this paper, we utilized the $N_{targets}$ values reported by Kubik *et al.*, who investigated the binding sites for four yeast remodelers of interest in this study, and explicitly quantified the number of mRNA gene promoters enriched for

each remodeler. Assuming that the +1 or -1 nucleosomes and the NDR together represent the main interaction substrates at promoter regions, this value of N_{targets} can be considered as a lower bound estimate. Accordingly, RSC binding is the most widespread ($N_{\text{targets}} = 3702$), SWI/SNF binds only a small subset ($N_{\text{targets}} = 466$), and INO80 ($N_{\text{targets}} = 1646$) and ISW2 ($N_{\text{targets}} = 1802$) each bind to approximately a third of all yeast promoters (Kubik et al., 2019). Because INO80 and ISW2 are also targeted to sites of DNA replication, as well as tDNA and ribosomal DNA loci (Cutler et al., 2018; Gelbart, Bachman, Delrow, Boeke, & Tsukiyama, 2005; Shimada et al., 2008), the total N_{targets} for each remodeler is likely to be larger than the values we utilized.

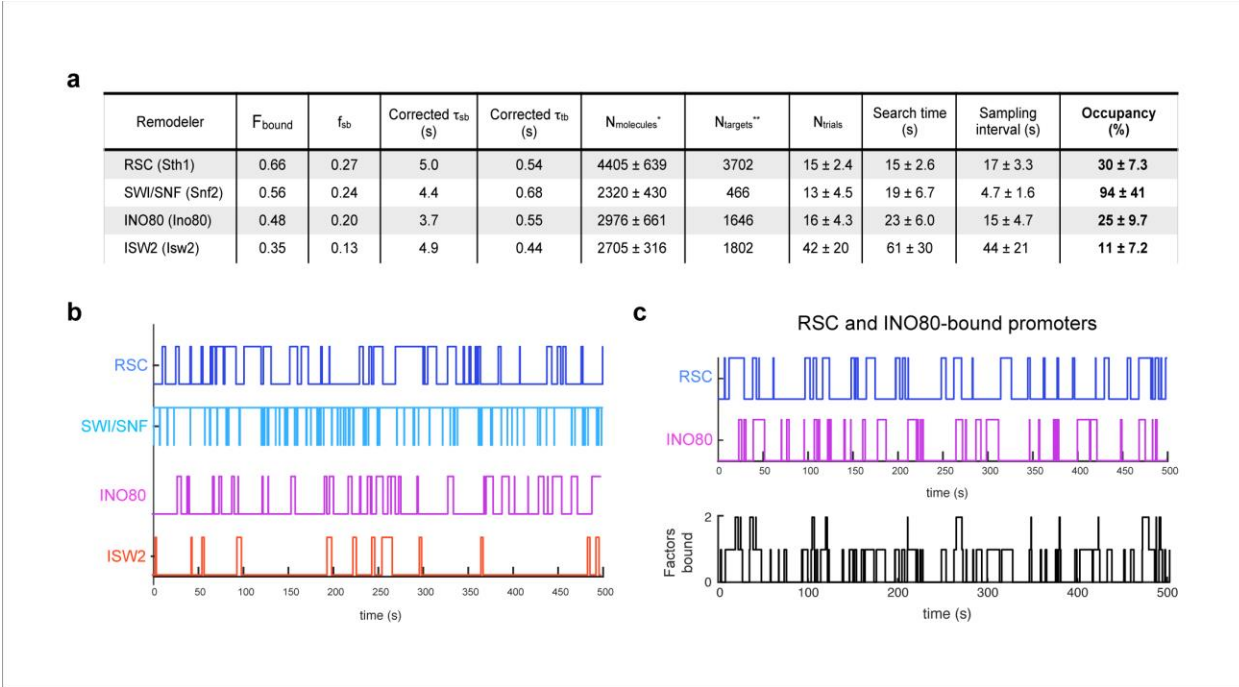


Figure 7. Remodelers show substantial temporal occupancies at chromatin targets.

(A) Key parameters measured in this study and acquired from the literature (Ho et al., 2018; Kubik et al., 2019) are used to calculate occupancy levels for gene promoter-acting remodelers. (B) Time trace simulations of temporal occupancy for individual remodelers at a target promoter region based on average τ_{sb} and sampling interval. Top and bottom bars represent occupied (on) and vacant (off) states, respectively, and vertical lines depict transitions between the two states. (C) Time trace simulations of occupancy at a RSC- and INO80-bound promoter region based on average τ_{sb} and sampling interval. Individual time trace simulations are shown above, and the cumulative simulated occupancy plot (black) shows either one or both remodelers bound in the time course of 500 s.

Figure supplement 1. Time trace simulations of temporal occupancies at promoters bound by multiple remodelers, and analysis of CHD1 DNA-binding mutant.

To calculate occupancy values, we used the T_{search} (search time), the time it takes for a molecule to go from one stable target site to the next [i.e. time bound non-specifically plus time in free diffusion], the SI (sampling interval) [i.e. the time between initial binding of one molecule and binding of the second molecule], and the estimated values for $N_{\text{molecules}}$ and N_{targets} per cell (Figure 7A; see Methods). RSC shows substantial occupancy ($30 \pm 7.3\%$) at stably bound chromatin targets, despite its short residence time (T_{sb}) of 5.0 ± 0.7 s. Thus, rather than individual RSC molecules residing for long periods of time, the high occupancy rate can be attributed to the short T_{search} (15 ± 2.6 s) and comparable SI (17 ± 3.3 s) values coupled to high $N_{\text{molecules}}$ (>4000) (Figure 7A). SWI/SNF exhibits the highest occupancy ($94 \pm 41\%$) among the four remodelers, consistent with the highest raw ChEC signals reported for Swi3 (Kubik et al., 2019). Strikingly, our estimate indicates that SWI/SNF also maintains its occupancy at target sites by coupling short residence time (4.4 ± 1.2 s) with short SI (4.7 ± 1.6 s) (Figure 7A).

We next assessed the occupancy values for INO80 and ISW2, which oppose the actions of RSC and SWI/SNF. Comparable to RSC, INO80 displays substantial occupancy ($25 \pm 9.7\%$) at its targets while ISW2 displays a lower occupancy ($11 \pm 7.2\%$). INO80 exhibits short T_{search} (23 ± 6.0 s) and SI (15 ± 4.7 s) values, while ISW2 has a relatively longer T_{search} (61 ± 30 s) and SI (44 ± 21 s) values (Figure 7A). Average time trace simulations of stably bound occupancies for each of the four remodelers over several hundred seconds (Figure 7B) show that at promoter regions targeted by multiple remodelers such as genes in ‘cluster IV’ enriched for RSC and INO80 (Kubik et al., 2019), the occupancy by any one remodeler is strikingly high, and more than one remodeler can simultaneously engage a promoter repeatedly over several minutes (Figure 7C; see also Figure 7-figure supplement 1A,B). (Note that our calculated promoter occupancy values for INO80 and ISW2 represent an upper limit and are subject to revision depending on the extent of remodeler binding to sites of DNA replication or repair).

DISCUSSION

Imaging chromatin remodeler diffusion by the fast-tracking mode in yeast shows that they bind to chromatin at substantial frequencies [F_{bound} : 35 - 66%], and with a notable population [21 - 30%] displaying intermediate D values resulting from transitions between bound and free states (Figure 1-3). This suggests remodelers frequently undergo highly short-lived chromatin interactions and is consistent with our slow-tracking measurements of transient-binding frequency (f_{tb} : 73 - 87%) (Figure 4), and with FRAP and FCS measurements of over-expressed mammalian ISWI (Erdel, Schubert, Marth, Längst, & Rippe, 2010). The high frequency of transient interactions, and direct evidence for transitioning trajectories is also consistent with the model of 1D-3D facilitated diffusion, a proposed mechanism to increase the target search efficiency of nuclear proteins (Von Hippel & Berg, 1989),

By slow-tracking, two chromatin-associated populations, 'stable-binding' and 'transient-binding', were observed for all six remodelers. Previous SMT studies on the mammalian Sox2 and yeast Ace1 transcription factors showed that stable-binding subpopulation represent interactions with cognate target sequences (Chen et al., 2014; Mehta et al., 2018). Comparable to reported values for the Rsc2 subunit of RSC and the yeast transcription factors, Ace1 and Gal4 (Donovan et al., 2019; Mehta et al., 2018), all imaged remodelers show stable and transient residence times of 4-7 s and 0.4-0.7 s, respectively. Furthermore, the effect of mutating the DNA-binding domain of CHD1 monomer (Ryan, Sundaramoorthy, Martin, Singh, & Owen-Hughes, 2011; Tran, Steger, Iyer, & Johnson, 2000) results in a 3-fold reduction in the τ_{sb} value (from 7.2 ± 3.3 to 2.4 ± 0.7 s) (Figure 7-figure supplement 1C,D). Unlike sequence-specific transcription factors, a complete loss of stable-binding would not be expected for remodeling complexes, whose recruitment relies on multiple interactions with gene-specific transcription factors, histone modification recognition domains, and interaction with components of the transcription machinery (Becker & Workman, 2013). Indeed, we speculate that the multiplicity of interaction motifs has a central role in the unusual diffusive behaviors shown by chromatin remodelers.

Importantly, the fast dissociation rates of remodelers are facilitated by ATP hydrolysis. Five tested ATPase-dead mutants (for ISW2, ISW1, CHD1) show two-fold or greater increase in their stable-binding residence times (Figure 5C-F), highlighting a new role of ATP-utilization in coupling nucleosome remodeling to rapid enzyme dissociation from chromatin. This also suggests that their mean residence times can reflect timescales for the diverse reactions performed by remodeling enzymes on chromatin *in vivo*. Assuming that the +1 or -1 nucleosomes and the NDR are the main targets for promoter-acting RSC, SWI/SNF, INO80 and ISW2, their 4-7 s stable residence time would include time for diffusion on the NDR as well as time expended for nucleosome remodeling. Biochemical studies have shown that remodelers undertake small translocation steps with remodeling rates of a few bp/sec (Blosser, Yang, Stone, Narlikar, & Zhuang, 2009; Deindl et al., 2013; Harada et al., 2016; Qiu et al., 2018; Sabantsev, Levendosky, Zhuang, Bowman, & Deindl, 2019). For example, with an enzymatic rate of 2 bp/s for ISWI (Blosser et al., 2009), an ISWI stable-binding event would allow octamer sliding by roughly 12 bp, which is within range of *in vivo* nucleosome position changes after conditional inactivation of RSC, SWI/SNF, INO80 and ISW2 (Ganguli et al., 2014; Kubik et al., 2019).

Under our imaging conditions, the chromatin-bound populations of the six remodelers exhibit higher mobility than H2B measured for bulk incorporated histones (Figure 6A-C). We further showed that this enhanced mobility is dependent on the ATPase domain. Mutations in the ISW1, ISW2, and CHD1 Walker A motif implicated in nucleotide binding (Singleton et al., 2007) substantially decreases *in vivo* mobility. Further analysis of mutations in the CHD1 and ISW2 Walker B motif, implicated in ATP hydrolysis [but not ATP binding] (Singleton et al., 2007), displays a milder decrease of its chromatin mobility, suggesting that nucleotide binding is largely sufficient for promoting diffusion for the two remodelers. Previous observations for other DNA-binding ATPase enzymes have noted ATP binding-dependent, hydrolysis-independent 1D diffusion or sliding on DNA (Cho et al., 2012; Mazur, Mendillo, & Kolodner, 2006; Tóth, Bollins, & Szczelkun, 2015), suggesting that this mode of diffusion to enhance target search may be shared among remodelers. In addition, RSC and *Drosophila* ISWI remodelers undergo ATP

hydrolysis-dependent translocation on ssDNA and dsDNA in vitro (Saha, Wittmeyer, & Cairns, 2005; Whitehouse, Stockdale, Flaus, Szczelkun, & Owen-Hughes, 2003), with processivities of 20-70 bp/translocation event (Fischer, Saha, & Cairns, 2007; Saha et al., 2005; Sirinakis et al., 2011; Whitehouse et al., 2003). Finally, the absence of any change in ISW1 chromatin-bound mobility upon treatment with a general transcription inhibitor thiolutin rules out transcription *per se* as a source of enhanced remodeler diffusion (Figure 6-figure supplement 1B). In all, our results suggest that chromatin remodelers use the catalytic ATPase not only for nucleosome remodeling but also to enhance target search kinetics by promoting 1D diffusion on chromatin and rapid detachment after reaction.

Yeast promoter regions can be classified into different groups enriched either for no remodeler or a combination of RSC, SWI/SNF, INO80 and ISW2, with about half of promoters genome-wide harboring at least two distinct remodelers that harbor nucleosome pushing and pulling activities relative to the NDR (Kubik et al., 2019). At promoter regions where opposing remodelers bind, we expect a consecutive “tug-of-war” between the pushing and pulling activities, in which successive engagements would ultimately result in fine-tuning the steady-state nucleosome position, with the final outcome dependent on remodeler occupancy and nucleosome remodeling activity. Based on occupancy estimates, two remodelers may be found to simultaneously engage promoter chromatin (Figure 7C, Figure 7-figure supplement 1A,B), but steric considerations likely preclude two remodelers binding to the same nucleosome or the same face of a nucleosome. Alternatively, at promoter regions where none or only one remodeler binds, other mechanisms are likely to have more substantial roles in nucleosome positioning. These include the sequence-dependent bendability of promoter DNA as well as the binding of general regulatory factors (GRFs), such as Reb1, Abf1, and Rap1, acting as barriers to nucleosome mobility (Struhl & Segal, 2013).

A temporal model for nucleosome remodeling at NDRs

By integrating our live-cell SMT measurements with available genome-wide localization and protein expression data, we estimate temporal occupancies ranging from 11 ± 7.2 to $94 \pm 41\%$ for RSC, SWI/SNF, INO80, and ISW2 at target promoter regions including the NDR and flanking nucleosomes. Our findings of highly dynamic and frequent remodeler-nucleosome interactions are consistent with recent genomics studies showing substantial changes in nucleosome positions upon rapid, conditional inactivation of remodelers in yeast and mammalian systems (Iurlaro et al., 2021; Klein-Brill et al., 2019; Kubik et al., 2019; Schick et al., 2021). Accordingly, we envision a nucleosome remodeling cycle at promoters in which remodeler combinations undergo frequent association, ATP-dependent mobilization and dissociation from chromatin to dynamically fine-tune -1 and +1 nucleosome positions (Figure 8).

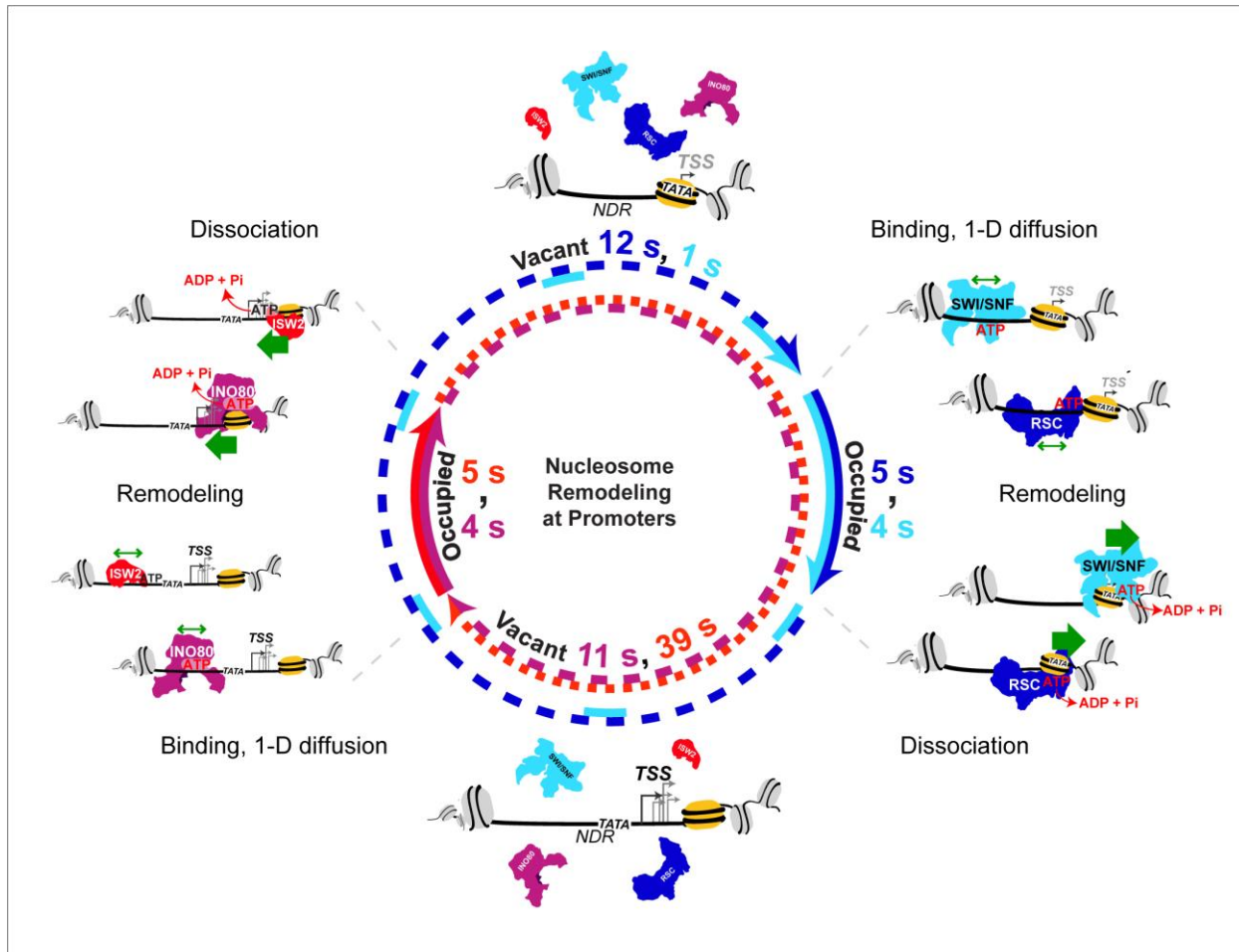


Figure 8. Nucleosome remodeling at promoters.

Model for nucleosome remodeling cycle at a gene promoter region targeted by RSC, SWI/SNF, INO80, and ISW2. The promoter region transitions between remodeler-occupied [solid arrow] and remodeler-vacant [dashed arrow] states, and their mean durations are indicated. After association with the NDR, remodelers undergo 1-D diffusion on chromatin facilitated by ATP binding, resulting in higher chromatin-associated mobility. Upon engaging a nucleosome substrate [e.g. the +1 nucleosome], RSC or SWI/SNF uses the energy of ATP hydrolysis to ‘push’ the nucleosome away from the NDR and INO80 or ISW2 to ‘pull’ the nucleosome into the NDR. ATP hydrolysis facilitates remodeler dissociation, and the promoter region becomes vacant for other factor interactions. The order of remodeler visitation is arbitrary, and simultaneous co-occupancy within the NDR can occur (see text for details).

We anticipate stochastic recruitment of RSC, SWI/SNF, INO80 and ISW2 to their target promoter regions. RSC recognizes general promoter characteristics, such as the long DNA stretch of the NDR (Wagner et al., 2020), histone acetylation marks potentially read by 8 bromodomains in four RSC subunits (Josling, Selvarajah, Petter, & Duffy, 2012), and the Rsc3 DNA-binding sequence motif found in several hundred promoters (Badis et al., 2008). These recruitment mechanisms likely account for RSC enrichment

at the majority of yeast promoters [3702/5040] (Kubik et al., 2019). For SWI/SNF recruitment to a minority of yeast promoters [466/5040 promoters], extensive studies have shown interactions with gene-specific transcription factors (Cosma, Tanaka, & Nasmyth, 1999; Neely et al., 1999; Peterson & Workman, 2000; Yudkovsky, Logie, Hahn, & Peterson, 1999). ISW2 also interacts with transcription factors such as Ume6 (Goldmark, Fazzio, Estep, Church, & Tsukiyama, 2000), but overall, less is known about the recruitment mechanisms for INO80 and ISW2, presenting opportunities for future studies.

Upon binding within the accessible NDR, RSC or SWI/SNF undergoes 1-D diffusion in an ATP-dependent manner, manifesting higher chromatin-associated mobility. On engagement with either flanking nucleosome substrate [+1 nucleosome shown], RSC or SWI/SNF uses the energy of ATP hydrolysis to reposition the nucleosome away from NDR, enlarging NDR length. Importantly, this remodeling activity also facilitates RSC or SWI/SNF dissociation. Subsequent stochastic recruitment of INO80 or ISW2, ATP-dependent 1-D diffusion, and nucleosome engagement remodels the nucleosome to move in the opposing direction and narrow the NDR, coupled with remodeler dissociation. Cycles of sequential or simultaneous binding and activity by the four remodelers with their similar dwell times (4-5 s) and varying sampling intervals (5-44 s) provides a dynamic temporal window of accessibility for promoter chromatin.

In a related study (Nguyen et al., 2021), the average promoter occupancy of the yeast PIC that forms upstream and overlapping the +1 nucleosome was found to be in the range of 10%, i.e. on the same order of magnitude but lower than three of four remodelers examined. Similar to chromatin remodelers, a full PIC lasts only several seconds before dissociation from chromatin, but the average promoter is vacant for ~100 seconds before PIC reformation. Thus, we suggest that there may be robust and dynamic competition between PIC components and mobilized NDR-flanking nucleosomes with chromatin exposure of key promoter elements such as the TATA box occurring for only a limited time window allowing proper assembly of downstream PIC components. This temporally positioned +1 nucleosome would enable Pol II to scan and

start transcription at the proper, canonical TSS. In this way, the dynamic interactions of remodeling enzymes with their promoter targets provides a temporal, chromatin accessibility-based regulatory mechanism for eukaryotic transcription.

Taken together, our SMT study elucidates the dynamic behaviors of this family of nuclear proteins and offers insights into additional kinetic functions for the remodeling ATPase and the timescales that govern nucleosome repositioning in relation to transcription events. It is notable that an independent study from the Verrijzer laboratory (Tilly et al. 2021) found that the *Drosophila* Brahma (BRM) remodeler also displays dependence on ATP utilization by the catalytic ATPase for dynamic mobility and remodeler dissociation in live *Drosophila* cells. For INO80 and ISW2, it would be of interest to distinguish their diffusive behaviors specific to DNA replication in cells undergoing S phase, and to DNA repair in the presence of DNA damaging agents. Outstanding questions also include determining the kinetic parameters for other chromatin regulators such as histone acetyltransferases, methyltransferases, histone de-modification enzymes, and histone chaperones, to gain a comprehensive view of the overall competition for engagement of promoter-proximal nucleosomes, their effects on nucleosome positioning and the dynamics of transcription complexes. Our findings in live cells provide a temporal framework for further testing of proposed models and should facilitate development of in vitro single-molecule assays that allow direct observation of physical and functional interactions between transcription regulators, chromatin, and the transcription machinery.

MATERIALS AND METHODS

Key Resources Table				
Reagent type (species) or resource	Designation	Source or reference	Identifiers	Additional information
strain, strain background (<i>S. cerevisiae</i>)	Full list of yeast strains is presented in Supplement ary file 1.			
recombinant DNA reagent	pBS-SK-Halo-NatMX (plasmid)	(Ranjan et al., 2020)		
recombinant DNA reagent	pUG72 (plasmid)	Euroscarf, Germany	pUG72 (P30117)-Euroscarf	
sequence-based reagent	Full list of oligonucleotides is presented in Supplement ary file 2.			
chemical compound, drug	JF552-HaloTag ligand	(Zheng et al., 2019b)	N/A	
chemical compound, drug	JF646-HaloTag ligand	(Grimm et al., 2015a)	N/A	
chemical compound, drug	#1.5 Micro Coverglass – 25 mm Diameter	Electron Microscopy Sciences	72225-01	
software, algorithm	ImageJ (1.52p)	ImageJ	RRID:SCR_003070 https://imagej.net/	

software, algorithm	Diatrack 3.05	(Vallotton & Olivier, 2013)	http://www.diatrack.org/index.html	
software, algorithm	GraphPad Prism version 8.4.2	GraphPad Software, Inc.	RRID:SCR_002798 http://www.graphpad.com	
software, algorithm	Sojourner package	Carl Wu lab	https://rdrr.io/github/sheng-liu/sojourner/	
software, algorithm	Spot-On	(Hansen et al., 2018)	https://spoton.berkeley.edu/	
software, algorithm	vbSPT	(Persson et al., 2013)	http://vbspt.sourceforge.net/	
software, algorithm	Radius of confinement calculation	(Lerner et al., 2020)	https://data.mendeley.com/datasets/wctzwpp9h2/2	
software, algorithm	Custom Matlab script	This paper, Mendeley Data	http://dx.doi.org/10.17632/ydwcx9yhpp.2	

Yeast strains

All *Saccharomyces cerevisiae* strains used in this study are isogenic derivatives of W303 strain carrying *pdr5*Δ for efficient JF ligand labeling, and are listed in Supplementary file 1. HaloTag was fused to the C-terminus of the protein of interest using standard methods for yeast transformation, using pBS-SK-Halo-NatMX plasmid (Ranjan et al., 2020). Point mutations were introduced by either the traditional “pop-in pop-out” (Rothstein, 1991) or the “50:50” method (Horecka & Davis, 2014), using pUG72 plasmid (P30117, Euroscarf, Germany), and list of primers are provided in Supplementary file 2.

Yeast Growth Assays

The cell growth of strains carrying HaloTag fusion constructs were compared to their derived parental genotype. The strains grown to saturation in YPAD (Yeast Extract-

Peptone-Dextrose + 40 mg/L Ade-SO₄) were serially diluted (5-fold dilutions) on YPAD plates. Plates were imaged after 48 or 72 h growing at 3 different temperatures (25°C, 30°C, and 38°C).

Cell Lysate Preparation to check integrity of HaloTag fusion proteins

Yeast cultures growing at early log phase (OD₆₀₀ 0.2) were treated with JF646 dye at a saturating dye concentration of 20 nM JF646 (Grimm et al., 2015a) was used instead of JF552 for better dye labeling (Ranjan et al., 2020). Yeast protein extract was prepared using the NaOH method (Amberg, Burke, & Strathern, 2006). Total protein concentration was measured using the Bradford Assay, and 45 ng of total protein was loaded per well in SDS-PAGE. Gels were imaged on Tecan 5 scanner, with Cy5 excitation. After imaging, gels were stained with Coomassie dye for loading control.

Yeast culture preparation for single molecule imaging

Yeast cultures growing in Synthetic Complete Medium (0.79 g/L Complete Supplement Mixture [CSM] Powder, Sunrise Science Products, Cat. No. 1001-010; 6.7 g/L Yeast nitrogen base without amino acids, BD Difco, Cat. No. DF0919-15-3; 2% (w/v) dextrose; 40 mg/L Adenine hemisulfate) were treated with dyes at early log phase (D₆₀₀ 0.2 - 0.3) for 2 h. For fast-tracking, saturating dye concentrations ranging from 10 to 20 nM JF552 (Zheng et al., 2019a) were used depending on factor abundance. For slow-tracking, we used 5 - 7.5 nM JF552. In some instances, we also added JF646 (~5 nM) to visualize nuclear fluorescence without JF552 excitation and to partially reduce JF552 labelling. Cells were harvested around mid-log phase by brief centrifugation (3500 rpm for 2 min), washed at least 3 times, and finally resuspended in CSM medium. Resuspended cells were loaded on Concanavalin A-treated coverslip (#1.5 Micro Coverglass -25 mm Diameter, Electron Microscopy Sciences, Cat. No. 72225-01) assembled on imaging cell chamber (Invitrogen, Cat. No. A7816), where coverslips were flamed prior to the treatment in order to reduce single-to-noise background. After immobilization and additional washing, ~1.5 mL of fresh medium was added to the chamber in which the cells are bathed continually for the duration of the imaging session (~2 h). Comparison

of results from the first and second halves of an imaging session shows no substantial differences (Figure 1-Figure supplement 3A).

Live cell, single molecule imaging using wide-field microscopy

Microscope setup: All yeast imaging was performed using a custom-built Zeiss widefield microscope (Axio Observer Z1) with a 150X glycerin immersion objective (NA 1.35) as previously described (Ranjan et al., 2020). Data was acquired with EM-CCD (Hamamatsu C9100-13) camera with FF01-750/SP and NF03-405/488/561/635E quad-notch filters for a final x-y pixel size of 107 nm. All imaging was performed with a single excitation channel. For JF552 dye excitation, 555 nm laser (Crystalaser) at (TTL pulsed) with 561 beam-splitter and 612/69 nm filter was used. For JF646 dye excitation, a 639 nm laser with 648 beamsplitter and 676/29 nm filter was used. Microscope manipulations (i.e. Z-focus, X/Y translation, filter cube switch) was performed by Zen software (Zeiss, Germany) and camera and data acquisition was controlled by HCLImage software (Hamamatsu Photonics, Japan).

Data acquisition

After yeast immobilization, the asynchronous cells representing all phases of the cell cycle were imaged for around 2 h at room temperature.

Fast tracking: Movies with 10 ms exposure/frame were recorded with continuous 555 nm laser irradiation at $\sim 1 \text{ kW/cm}^2$. A field of view of 128 x 128 pixels was used to capture 4-6 yeast nuclei. Single-molecule imaging was performed using dSTORM (direct stochastic optical reconstruction microscopy) (Heilemann et al., 2008; Rust, Bates, & Zhuang, 2006). Each movie begins with global nuclear fluorescence on laser excitation of essentially all JF552-labelled molecules before photoconversion to a dark, non-fluorescent state. The duration of the initial excitation pulse which pushes fluorescent JF552 to the dark state is $\sim 10 \text{ s}$, depending on the density of labeled Halo-proteins, which is a function of protein expression and dye labeling concentration adjusted for the specific protein. Once in the dark state, JF552 spontaneously and stochastically converts back to the fluorescent state (Grimm et al., 2015b; Zheng et al., 2019a). This conversion is sufficiently slow such that mostly one JF552 molecule per

yeast nucleus is fluorescent at any given time during data acquisition, allowing for an unambiguous spatio-temporal record of single JF552-labeled proteins. To ensure that we can harvest a ‘substack’ of at least 5000 frames (10 ms/frame) (See Single molecule image analysis), we routinely record movies of ~1.5 min. About 40 movies were acquired per imaging session, and 2 [or 3 for ISW2] biological replicates were obtained for each sample.

Under fast-tracking conditions, cells displayed no detectable cellular damage and underwent normal bud growth and cell division when examined every 30 minutes up to 3 hours (Nguyen et al., 2021). Furthermore, we did not observe any substantial difference between the first and second half of each movie (Figure 1-Figure supplement 3B).

Slow tracking: Movies with 250 ms exposure/frame were acquired using continuous 555 nm laser irradiation at 0.05 kW/cm² (5% of fast-tracking power) for sufficient signal-to-noise while minimizing photobleaching. A focal plane of 256 x 256 pixels was used to capture 15-20 yeast nuclei. In the beginning of each movie, the 639 nm excitation channel was briefly used to fine-tune the focus, and then immediately switched to 555 nm excitation to start data acquisition. Upon 555 nm laser illumination, we record ~5 min movies starting with fluorescent JF552 pushed to the dark state for > 30 s, followed by single-molecule imaging of at least 750 frames at 250 ms/frame. 15-20 movies were taken per imaging session, with 2 or 3 biological replicates for wildtype and 2 to 4 biological replicates for mutant strains.

Single molecule image analysis

For each raw movie, we first manually selected a ‘substack’ where ~1 single molecule per nucleus per frame was observed in order to minimize tracking errors resulting from connecting different molecules as one trajectory. Substack lengths of 5000 frames (50 s) and 750 frames (3.125 min) were selected for fast and slow tracking movies, respectively, using ImageJ (1.52p) custom-written script. The substacks were then applied to the Diatrack software (ver. 3.05, <http://www.diatrack.org/index.html>) to localize the centroid of PSF (point spread function) by Gaussian fitting over the

fluorescence intensity to sub-pixel resolution (Thompson, Larson, & Webb, 2002; Yildiz et al., 2003) and track single particles (Vallotton & Olivier, 2013). For localization, the following parameters were applied: Remove dim: 75 - 85, Remove blurred: 0.1, Activate High Precision mode: ON (HWHM=1 pixel). For tracking, we used max jump of '6' (642 nm) and '3' pixels (321 nm) for fast and slow tracking datasets, respectively. Furthermore, we masked the nuclear regions based on the maximum intensity Z-projection of the selected substacks to filter out trajectories found outside of the nucleus in the subsequent analysis steps. The Diatrack output file containing information about the x, y coordinate and frame number were then applied for further downstream analysis.

Fast tracking:

MSD-based diffusion coefficient histograms: All “masked” trajectories with at least 5 displacements were analyzed, using the lab custom-written R package, Sojourner (<https://rdr.io/github/sheng-liu/sojourner/>). Briefly, for each trajectory, MSD plot for time lags from 2 to 5 Δt ($\Delta t = 10$ ms) were generated, then fit to linear regression (filtering out $R^2 < 0.8$ plots). From the slope, the diffusion coefficient was calculated as (where d is the number of dimensions, or 2):

$$D = \frac{1}{2d} \times \frac{MSD(dt)}{dt}$$

Spot-On (Hansen et al., 2018): All “masked” trajectories with at least 2 displacements were analyzed. The following parameters were applied for Jump Length Distribution: Bin width (μm): 0.01, Number of time-points: 6, Jumps to consider: 4, Use entire trajectories No, Max jump (μm): 2. Additionally, the following parameters were applied for 2-state Model Fitting: D_{bound} ($\mu\text{m}^2/\text{s}$): 0.0005-0.1, D_{free} ($\mu\text{m}^2/\text{s}$): 0.15-25, F_{bound} : 0-1, Localization error (μm): Fit from data (0.01-0.1), dZ (μm): 0.6, Use Z correction, Model Fit: CDF, Iterations: 3.

vbSPT (variational Bayesian) HMM (Persson et al., 2013): All “masked” trajectories with at least 2 displacements were analyzed. The following parameters were used to run

vbSPT-1.1.3 to classify each displacement into two states, “Bound” or “Free” (Hansen *et al.*, 2020, <https://gitlab.com/anders.sejr.hansen/anisotropy>): timestep= 0.01; dim= 2; trjLmin= 2; runs= 3; maxHidden= 2; stateEstimate= 1; bootstrapNum=10; fullBootstrap= 0; init_D = [0.001, 16]; init_tD = [2, 20]*timestep; and default prior choices according to (Persson *et al.*, 2013).

Then each trajectory was sub-classified as “Bound only” if all displacements are classified as bound state; “Free only” if all displacements are classified as free state; and “Transitioning” if the trajectory contains both bound and free displacements with at least two consecutive displacements in each state. To validate that the transitioning trajectories consist of bound and free states, we calculated and compared the displacement length between “bound only” and bound segments of transitioning trajectories, and between “free only” and free segments of transitioning trajectories. Finally, the sub-classified trajectories were used to regenerate the diffusion coefficient histograms.

Radius of confinement: All “masked” trajectories with at least 4 displacements were analyzed, as described previously (Lerner *et al.*, 2020). To determine the radius of confinement exhibited by chromatin-bound molecules, we analyzed trajectories classified as “bound only” by vbSPT (as described above). Since many confined trajectories with low D do not pass the $R^2 \geq 0.8$ filter, we used all trajectories whose MSD plots passed the more lenient $R^2 \geq 0.1$ filtering. The MSD plot was then fit to the circular confined diffusion model:

$$MSD_{circle} = R^2 \cdot \left(1 - e^{\frac{-4 \cdot D \cdot t_{lag}}{R^2}} \right)$$

where R is the radius of confinement, D is the short-term diffusion coefficient. Specifically, the first 10 time points of the MSD plot were used to fit to the model, and trajectories with squared norm of residual (RSS) higher than 10^{-5} and Rc higher than 300 nm were discarded.

Slow tracking:

Residence times: Using Sojourner package, the apparent lifetimes (temporal length of trajectories) were determined for all “masked” trajectories lasting at least 3 frames. To account for blinking or mislocalizations, we allowed for gaps up to 2 frames between two localizations and linked them as one trajectory if they were less than 3 pixels apart. 1-CDF curves were generated and fit to a double exponential decay model:

$$P(t) = f_{sb} e^{-k_{sb}t} + f_{tb} e^{-k_{tb}t}$$

where k_{sb} and k_{tb} correspond to dissociation rates for stable- and transient-binding events, respectively, and $1 = f_{sb} + f_{tb}$ for the 2 components.

The apparent k_{sb} and k_{tb} values are affected by technical and imaging limitations such as photobleaching and chromatin movements. To correct for this bias, we used apparent dissociation rates of H2B imaged under same conditions as described previously (Hansen et al., 2017). The corrected residence times for stable- (τ_{sb}) and transient binding (τ_{tb}) were calculated as follows:

$$\tau_{sb} = \frac{1}{k_{sb} - k_{sb,H2B}}$$

$$\tau_{tb} = \frac{1}{k_{tb} - k_{sb,H2B}}$$

Apparent diffusion coefficient values for stably bound trajectories: All “masked” trajectories lasting at least 5 frames (not allowing for gaps) were analyzed, using Sojourner package. For each trajectory, MSD plot for time lags from 2 to 5 Δt ($\Delta t = 10$ ms) were generated, then fit to linear regression (filtering out $R^2 < 0.8$ plots). From the slope, the diffusion coefficient was calculated as (where d is the number of dimensions, or 2):

$$D = \frac{1}{2d} \times \frac{MSD(dt)}{dt}$$

Occupancy calculation

To calculate temporal occupancy, we integrated approaches from previous studies (Chen et al., 2014; Loffreda et al., 2017; Tatavosian et al., 2018).

Search time (τ_{search}) is the average time it takes for a molecule to go from one specific site to its next specific site. The two specific binding events (lasting for τ_{sb}) are interspersed by a number of trials (N_{trials}) binding to non-specific sites (lasting for τ_{tb}). τ_{free} is the average free time between 2 binding events. Assuming equal probability of binding to all specific and non-specific sites, the search time is calculated as follows:

$$\tau_{\text{search}} = N_{\text{trials}} \times \tau_{\text{tb}} + (N_{\text{trials}} + 1) \times \tau_{\text{free}}$$

N_{trials} depends on the ratio of number of non-specific (N_{ns}) to specific sites (N_{s}), or r_{s} :

$$N_{\text{trials}} = \frac{N_{\text{s}} + N_{\text{ns}}}{N_{\text{s}}} = 1 + r_{\text{s}}$$

Here, r_{s} can be determined based on two assumed scenarios for bound molecules observed during slow tracking (as described in Nguyen et al., 2021). First, f_{sb} determined by slow tracking depends on the time a molecule spends bound to specific sites compared to nonspecific sites:

$$f_{\text{sb}} = \frac{N_{\text{s}} \times \tau_{\text{sb}}}{N_{\text{s}} \times \tau_{\text{sb}} + N_{\text{ns}} \times \tau_{\text{tb}}} = \frac{\tau_{\text{sb}}}{\tau_{\text{sb}} + r_{\text{s},1} \times \tau_{\text{tb}}}$$

Thus r_{s} is equal to:

$$r_{\text{s},1} = \frac{\tau_{\text{sb}}}{\tau_{\text{tb}}} \times \left(\frac{1}{f_{\text{sb}}} - 1 \right)$$

In the second scenario, f_{sb} depends on the probability that a free molecule binds to a specific site over all sites:

$$f_{\text{sb}} = \frac{N_{\text{s}}}{N_{\text{s}} + N_{\text{ns}}} = \frac{1}{1 + r_{\text{s},2}}$$

In this case r_{s} is:

$$r_{\text{s},2} = \frac{1}{f_{\text{sb}}} - 1$$

We take the average value calculated from the 2 proposed scenarios to finally determine r_{s} :

$$r_{\text{s}} = \frac{1}{2} \left(\frac{1}{f_{\text{sb}}} - 1 \right) \left(\frac{\tau_{\text{sb}}}{\tau_{\text{tb}}} + 1 \right)$$

In fast tracking, F_{bound} is percentage or fraction of the time a molecule spends bound to chromatin either specifically or non-specifically:

$$F_{bound} = \frac{N_{trials} \times \tau_{tb} + \tau_{sb}}{N_{trials} \times \tau_{tb} + \tau_{sb} + (N_{trials} + 1) \times \tau_{free}}$$

809 Thus τ_{free} is (in terms of r_s):

$$\tau_{free} = \frac{\frac{(1 + r_s) \times \tau_{tb} + \tau_{sb}}{F_{bound}} - (1 + r_s) \times \tau_{tb} - \tau_{sb}}{2 + r_s}$$

810 Using the values derived for r_s and τ_{free} , we then calculated the search time as shown
811 above.

812 Sampling interval (SI) is the time interval between two specific binding events at a given
813 site as described previously (Chen et al., 2014):

$$Sampling\ Interval\ (SI) = \frac{(\tau_{search} + \tau_{sb}) \times N_{targets}}{N_{molecules}}$$

814 We used $N_{targets}$ values presented by (Kubik et al., 2019). $N_{molecules}$ was determined as
815 the median and standard error values (Ho et al., 2018), and their standard error was
816 used for error propagation.

817 Finally, occupancy is the temporal probability that a given specific site is occupied by
818 the protein of interest:

$$Occupancy = \frac{\tau_{sb}}{SI}$$

819

820 **Target occupancy simulation**

821 Remodeler occupancy at a target promoter region was simulated as described
822 previously (Nguyen et al., 2021). Briefly, experimentally determined τ_{sb} and estimated
823 sampling interval (SI) values were used to simulate sequential promoter-occupied and
824 vacant states over the time trace (500 s). The duration for each occupied and vacant
825 state was randomly chosen from exponential distributions of the average τ_{sb} and (SI- τ_{sb})
826 values, respectively. For promoter regions targeted by multiple remodelers, each
827 remodeler was independently subject to the occupancy simulation, and the number of
828 any single or multiple remodeler(s) co-occupying each timepoint was calculated
829 throughout the time trace.

830

831 **ACKNOWLEDGEMENTS**

We thank Vu Q. Nguyen, Anand Ranjan, and Gaku Mizuguchi for experimental guidance at the initial stages of this project, Sun Jay Yoo, Yick Hin Ling and Taibo Li for computational assistance, Pascal Vallotton for support with Diatrack software, Jonathan Lerner, Ken Zaret, and Melike Lakadamyali for assistance with the Two-parameter single-molecule analysis, Slawomir Kubik and David Shore for advice on analysis of genomic data on remodeling enzymes, Toshio Tsukiyama and Brad Cairns for yeast strains, Anders Hansen and Greg Bowman for discussions, Wu lab members for helpful comments, and Peter Verrijzer for sharing a pre-print of his study. This study was supported by funds from a Korean Foundation for Advanced Studies Fellowship (J.M.K.), a Johns Hopkins Bloomberg Distinguished Professorship (C.W.) and National Institute of Health grant GM132290-01 (C.W.).

COMPETING INTERESTS

T.L. holds intellectual property rights related to Janelia Fluor dyes used in this publication. L.D.L. and Q.Z. are listed as inventors on patents and patent applications whose value might be affected by publication. US Patent 9,933,417 and Patent Application 2021/0085805 describing azetidine-containing fluorophores and variant compositions (with inventors Q.Z., L.D.L., and T.L.) are assigned to HHMI. The remaining authors declare no competing interests.

REFERENCES

- Albert, I., Mavrich, T. N., Tomsho, L. P., Qi, J., Zanton, S. J., Schuster, S. C., & Pugh, B. F. (2007). Translational and rotational settings of H2A.Z nucleosomes across the *Saccharomyces cerevisiae* genome. *Nature*. <https://doi.org/10.1038/nature05632>
- Almer, A., & Hörz, W. (1986). Nuclease hypersensitive regions with adjacent positioned nucleosomes mark the gene boundaries of the PHO5/PHO3 locus in yeast. *The EMBO Journal*, 5(10), 2681–2687. <https://doi.org/10.1002/j.1460-2075.1986.tb04551.x>
- Amberg, D. C., Burke, D. J., & Strathern, J. N. (2006). Yeast Protein Extracts. *Cold Spring Harbor Protocols*, 2006(1), pdb.prot4152. <https://doi.org/10.1101/pdb.prot4152>

Au, T. J., Rodriguez, J., Vincent, J. A., & Tsukiyama, T. (2011). ATP-Dependent Chromatin Remodeling Factors Tune S Phase Checkpoint Activity. *Molecular and Cellular Biology*, 31(22), 4454–4463. <https://doi.org/10.1128/mcb.05931-11>

Badis, G., Chan, E. T., van Bakel, H., Pena-Castillo, L., Tillo, D., Tsui, K., ... Hughes, T. R. (2008). A Library of Yeast Transcription Factor Motifs Reveals a Widespread Function for Rsc3 in Targeting Nucleosome Exclusion at Promoters. *Molecular Cell*, 32(6), 878–887. <https://doi.org/10.1016/j.molcel.2008.11.020>

Ball, D. A., Mehta, G. D., Salomon-Kent, R., Mazza, D., Morisaki, T., Mueller, F., ... Karpova, T. S. (2016). Single molecule tracking of Ace1p in *Saccharomyces cerevisiae* defines a characteristic residence time for non-specific interactions of transcription factors with chromatin. *Nucleic Acids Research*, 44(21), 1–12. <https://doi.org/10.1093/nar/gkw744>

Basu, S., Shukron, O., Ponjavic, A., Parruto, P., Boucher, W., Zhang, W., ... Laue, E. D. (2020). Live-cell 3D single-molecule tracking reveals how NuRD modulates enhancer dynamics. *BioRxiv*, 2020.04.03.003178. <https://doi.org/10.1101/2020.04.03.003178>

Becker, P. B., & Workman, J. L. (2013). Nucleosome remodeling and epigenetics. *Cold Spring Harbor Perspectives in Biology*. <https://doi.org/10.1101/cshperspect.a017905>

Blosser, T. R., Yang, J. G., Stone, M. D., Narlikar, G. J., & Zhuang, X. (2009). Dynamics of nucleosome remodelling by individual ACF complexes. *Nature*, 462(7276), 1022–1027. <https://doi.org/10.1038/nature08627>

Brahma, S., & Henikoff, S. (2019). RSC-Associated Subnucleosomes Define MNase-Sensitive Promoters in Yeast. *Molecular Cell*. <https://doi.org/10.1016/j.molcel.2018.10.046>

Chen, J., Zhang, Z., Li, L., Chen, B. C., Revyakin, A., Hajj, B., ... Liu, Z. (2014). Single-molecule dynamics of enhanceosome assembly in embryonic stem cells. *Cell*. <https://doi.org/10.1016/j.cell.2014.01.062>

Cheung, V., Chua, G., Batada, N. N., Landry, C. R., Michnick, S. W., Hughes, T. R., & Winston, F. (2008). Chromatin- and transcription-related factors repress transcription from within coding regions throughout the *Saccharomyces cerevisiae*

894 genome. *PLoS Biology*. <https://doi.org/10.1371/journal.pbio.0060277>

895 Cho, W. K., Jeong, C., Kim, D., Chang, M., Song, K. M., Hanne, J., ... Lee, J. B. (2012).
 896 ATP alters the diffusion mechanics of MutS on mismatched DNA. *Structure*.
 897 <https://doi.org/10.1016/j.str.2012.04.017>

898 Cosma, M. P., Tanaka, T., & Nasmyth, K. (1999). Ordered recruitment of transcription
 899 and chromatin remodeling factors to a cell cycle- and developmentally regulated
 900 promoter. *Cell*. [https://doi.org/10.1016/S0092-8674\(00\)80740-0](https://doi.org/10.1016/S0092-8674(00)80740-0)

901 Cutler, S., Lee, L. J., & Tsukiyama, T. (2018). Chromatin remodeling factors isw2 and
 902 ino80 regulate chromatin, replication, and copy number of the *Saccharomyces*
 903 *cerevisiae* ribosomal DNA locus. *Genetics*.
 904 <https://doi.org/10.1534/genetics.118.301579>

905 Deindl, S., Hwang, W. L., Hota, S. K., Blosser, T. R., Prasad, P., Bartholomew, B., &
 906 Zhuang, X. (2013). ISWI remodelers slide nucleosomes with coordinated multi-
 907 base-pair entry steps and single-base-pair exit steps. *Cell*, 152(3), 442–452.
 908 <https://doi.org/10.1016/j.cell.2012.12.040>

909 Donovan, B. T., Huynh, A., Ball, D. A., Patel, H. P., Poirier, M. G., Larson, D. R., ...
 910 Lenstra, T. L. (2019). Live-cell imaging reveals the interplay between transcription
 911 factors, nucleosomes, and bursting. *The EMBO Journal*.
 912 <https://doi.org/10.15252/embj.2018100809>

913 Erdel, F., Schubert, T., Marth, C., Längst, G., & Rippe, K. (2010). Human ISWI
 914 chromatin-remodeling complexes sample nucleosomes via transient binding
 915 reactions and become immobilized at active sites. *Proceedings of the National*
 916 *Academy of Sciences of the United States of America*.
 917 <https://doi.org/10.1073/pnas.1003438107>

918 Fischer, C. J., Saha, A., & Cairns, B. R. (2007). Kinetic model for the ATP-dependent
 919 translocation of *Saccharomyces cerevisiae* RSC along double-stranded DNA.
 920 *Biochemistry*. <https://doi.org/10.1021/bi700930n>

921 Fitzgerald, D. J., DeLuca, C., Berger, I., Gaillard, H., Sigrist, R., Schimmele, K., &
 922 Richmond, T. J. (2004). Reaction cycle of the yeast Isw2 chromatin remodeling
 923 complex. *EMBO Journal*. <https://doi.org/10.1038/sj.emboj.7600364>

924 Floer, M., Wang, X., Prabhu, V., Berrozpe, G., Narayan, S., Spagna, D., ... Ptashne, M.

925 (2010). A RSC/nucleosome complex determines chromatin architecture and
 926 facilitates activator binding. *Cell*. <https://doi.org/10.1016/j.cell.2010.03.048>
 927 Ganguli, D., Chereji, R. V., Iben, J. R., Cole, H. A., & Clark, D. J. (2014). RSC-
 928 dependent constructive and destructive interference between opposing arrays of
 929 phased nucleosomes in yeast. *Genome Research*.
 930 <https://doi.org/10.1101/gr.177014.114>
 931 Gasser, S. M. (2002). Nuclear architecture: Visualizing chromatin dynamics in
 932 interphase nuclei. *Science*. <https://doi.org/10.1126/science.1067703>
 933 Gelbart, M. E., Bachman, N., Delrow, J., Boeke, J. D., & Tsukiyama, T. (2005).
 934 Genome-wide identification of Isw2 chromatin-remodeling targets by localization of
 935 a catalytically inactive mutant. *Genes and Development*.
 936 <https://doi.org/10.1101/gad.1298905>
 937 Gelbart, M. E., Rechsteiner, T., Timothy, J., Tsukiyama, T., & Richmond, T. J. (2001).
 938 Interactions of Isw2 Chromatin Remodeling Complex with Nucleosomal Arrays :
 939 Analyses Using Recombinant Yeast Histones and Immobilized Templates
 940 Interactions of Isw2 Chromatin Remodeling Complex with Nucleosomal Arrays :
 941 Analyses Using Recombinant Yeast Hi. *Molecular and Cellular Biology*, (June
 942 2014). <https://doi.org/10.1128/MCB.21.6.2098>
 943 Goldmark, J. P., Fazzio, T. G., Estep, P. W., Church, G. M., & Tsukiyama, T. (2000).
 944 The Isw2 chromatin remodeling complex represses early meiotic genes upon
 945 recruitment by Ume6p. *Cell*. [https://doi.org/10.1016/S0092-8674\(00\)00134-3](https://doi.org/10.1016/S0092-8674(00)00134-3)
 946 Grimm, J. B., English, B. P., Chen, J., Slaughter, J. P., Zhang, Z., Revyakin, A., ... Lavis,
 947 L. D. (2015a). A general method to improve fluorophores for live-cell and single-
 948 molecule microscopy. *Nature Methods*. <https://doi.org/10.1038/nmeth.3256>
 949 Grimm, J. B., English, B. P., Chen, J., Slaughter, J. P., Zhang, Z., Revyakin, A., ... Lavis,
 950 L. D. (2015b). A general method to improve fluorophores for live-cell and single-
 951 molecule microscopy. <https://doi.org/10.1038/nmeth.3256>
 952 Gu, B., Swigut, T., Spencley, A., Bauer, M. R., Chung, M., Meyer, T., & Wysocka, J.
 953 (2018). Transcription-coupled changes in nuclear mobility of mammalian cis-
 954 regulatory elements. *Science*. <https://doi.org/10.1126/science.aao3136>
 955 Hansen, A. S., Amitai, A., Cattoglio, C., Tjian, R., & Darzacq, X. (2020). Guided nuclear

956 exploration increases CTCF target search efficiency. *Nature Chemical Biology*,
 957 16(3), 257–266. <https://doi.org/10.1038/s41589-019-0422-3>
 958 Hansen, A. S., Pustova, I., Cattoglio, C., Tjian, R., & Darzacq, X. (2017). CTCF and
 959 cohesin regulate chromatin loop stability with distinct dynamics. *ELife*, 6.
 960 <https://doi.org/10.7554/eLife.25776.001>
 961 Hansen, A. S., Woringer, M., Grimm, J. B., Lavis, L. D., Tjian, R., & Darzacq, X. (2018).
 962 Robust model-based analysis of single-particle tracking experiments with spot-on.
 963 *ELife*. <https://doi.org/10.7554/eLife.33125>
 964 Harada, B. T., Hwang, W. L., Deindl, S., Chatterjee, N., Bartholomew, B., & Zhuang, X.
 965 (2016). Stepwise nucleosome translocation by RSC remodeling complexes. *ELife*,
 966 5(FEBRUARY2016), 1–20. <https://doi.org/10.7554/eLife.10051>
 967 Hartley, P. D., & Madhani, H. D. (2009). Mechanisms that Specify Promoter
 968 Nucleosome Location and Identity. *Cell*. <https://doi.org/10.1016/j.cell.2009.02.043>
 969 Hauk, G., McKnight, J. N., Nodelman, I. M., & Bowman, G. D. (2010). The
 970 Chromodomains of the Chd1 Chromatin Remodeler Regulate DNA Access to the
 971 ATPase Motor. *Molecular Cell*. <https://doi.org/10.1016/j.molcel.2010.08.012>
 972 Heilemann, M., van de Linde, S., Schüttelz, M., Kasper, R., Seefeldt, B., Mukherjee, A.,
 973 ... Sauer, M. (2008). Subdiffraction-Resolution Fluorescence Imaging with
 974 Conventional Fluorescent Probes. *Angewandte Chemie International Edition*,
 975 47(33), 6172–6176. <https://doi.org/10.1002/ANIE.200802376>
 976 Heintzman, N. D., Stuart, R. K., Hon, G., Fu, Y., Ching, C. W., Hawkins, R. D., ... Ren,
 977 B. (2007). Distinct and predictive chromatin signatures of transcriptional promoters
 978 and enhancers in the human genome. *Nature Genetics*.
 979 <https://doi.org/10.1038/ng1966>
 980 Ho, B., Baryshnikova, A., & Brown, G. W. (2018). Unification of Protein Abundance
 981 Datasets Yields a Quantitative *Saccharomyces cerevisiae* Proteome. *Cell Systems*.
 982 <https://doi.org/10.1016/j.cels.2017.12.004>
 983 Horecka, J., & Davis, R. W. (2014). The 50:50 method for PCR-based seamless
 984 genome editing in yeast. *Yeast (Chichester, England)*.
 985 <https://doi.org/10.1002/yea.2992>
 986 Iurlaro, M., Stadler, M. B., Masoni, F., Jagani, Z., Galli, G. G., & Schübeler, D. (2021).

987 Mammalian SWI/SNF continuously restores local accessibility to chromatin. *Nature*
988 *Genetics*. <https://doi.org/10.1038/s41588-020-00768-w>

989 Izeddin, I., Récamier, V., Bosanac, L., Cissé, I. I., Boudarene, L., Dugast-Darzacq, C.,
990 ... Darzacq, X. (2014). Single-molecule tracking in live cells reveals distinct target-
991 search strategies of transcription factors in the nucleus. *ELife*, 2014(3), 1–27.
992 <https://doi.org/10.7554/eLife.02230>

993 Josling, G. A., Selvarajah, S. A., Petter, M., & Duffy, M. F. (2012). The role of
994 bromodomain proteins in regulating gene expression. *Genes*, 3(2), 320–343.
995 <https://doi.org/10.3390/genes3020320>

996 Klein-Brill, A., Joseph-Strauss, D., Appleboim, A., & Friedman, N. (2019). Dynamics of
997 Chromatin and Transcription during Transient Depletion of the RSC Chromatin
998 Remodeling Complex. *Cell Reports*. <https://doi.org/10.1016/j.celrep.2018.12.020>

999 Kubik, S., Bruzzone, M. J., Challal, D., Dreos, R., Mattarocci, S., Bucher, P., ... Shore,
1000 D. (2019). Opposing chromatin remodelers control transcription initiation frequency
1001 and start site selection. *Nature Structural and Molecular Biology*.
1002 <https://doi.org/10.1038/s41594-019-0273-3>

1003 Kubik, S., Bruzzone, M. J., Jacquet, P., Falcone, J. L., Rougemont, J., & Shore, D.
1004 (2015). Nucleosome Stability Distinguishes Two Different Promoter Types at All
1005 Protein-Coding Genes in Yeast. *Molecular Cell*.
1006 <https://doi.org/10.1016/j.molcel.2015.10.002>

1007 Kubik, S., O'Duibhir, E., de Jonge, W. J., Mattarocci, S., Albert, B., Falcone, J. L., ...
1008 Shore, D. (2018). Sequence-Directed Action of RSC Remodeler and General
1009 Regulatory Factors Modulates +1 Nucleosome Position to Facilitate Transcription.
1010 *Molecular Cell*. <https://doi.org/10.1016/j.molcel.2018.05.030>

1011 Lai, W. K. M., & Pugh, B. F. (2017a). Understanding nucleosome dynamics and their
1012 links to gene expression and DNA replication. *Nature Reviews Molecular Cell*
1013 *Biology*. <https://doi.org/10.1038/nrm.2017.47>

1014 Lai, W. K. M., & Pugh, B. F. (2017b). Understanding nucleosome dynamics and their
1015 links to gene expression and DNA replication. *Nature Reviews Molecular Cell*
1016 *Biology*, 18(9), 548–562. <https://doi.org/10.1038/nrm.2017.47>

1017 Lee, L., Rodriguez, J., & Tsukiyama, T. (2015). Chromatin remodeling factors Isw2 and

1018 Ino80 regulate checkpoint activity and chromatin structure in s phase. *Genetics*,
1019 199(4), 1077–1091. <https://doi.org/10.1534/genetics.115.174730>

1020 Lerner, J., Gomez-Garcia, P. A., McCarthy, R. L., Liu, Z., Lakadamyali, M., & Zaret, K. S.
1021 (2020). Two-Parameter Mobility Assessments Discriminate Diverse Regulatory
1022 Factor Behaviors in Chromatin. *Journal of Cleaner Production*.
1023 <https://doi.org/10.1016/j.molcel.2020.05.036>

1024 Lionnet, T., & Wu, C. (2021). Single-molecule tracking of transcription protein dynamics
1025 in living cells: seeing is believing, but what are we seeing? *Current Opinion in*
1026 *Genetics & Development*, *In press*. Retrieved from
1027 <https://www.journals.elsevier.com/current-opinion-in-genetics-and-development>

1028 Loffreda, A., Jacchetti, E., Antunes, S., Rainone, P., Daniele, T., Morisaki, T., ... Mazza,
1029 D. (2017). Live-cell p53 single-molecule binding is modulated by C-terminal
1030 acetylation and correlates with transcriptional activity. *Nature Communications*.
1031 <https://doi.org/10.1038/s41467-017-00398-7>

1032 Lusser, A., Urwin, D. L., & Kadonaga, J. T. (2005). Distinct activities of CHD1 and ACF
1033 in ATP-dependent chromatin assembly. *Nature Structural and Molecular Biology*,
1034 12(2), 160–166. <https://doi.org/10.1038/nsmb884>

1035 Maier, V. K., Chioda, M., Rhodes, D., & Becker, P. B. (2008). ACF catalyses
1036 chromatosome movements in chromatin fibres. *EMBO Journal*.
1037 <https://doi.org/10.1038/sj.emboj.7601902>

1038 Marshall, W. F., Straight, A., Marko, J. F., Swedlow, J., Dernburg, A., Belmont, A., ...
1039 Sedat, J. W. (1997). Interphase chromosomes undergo constrained diffusional
1040 motion in living cells. *Current Biology*. [https://doi.org/10.1016/S0960-](https://doi.org/10.1016/S0960-9822(06)00412-X)
1041 [9822\(06\)00412-X](https://doi.org/10.1016/S0960-9822(06)00412-X)

1042 Mavrich, T. N., Ioshikhes, I. P., Venters, B. J., Jiang, C., Tomsho, L. P., Qi, J., ... Pugh,
1043 B. F. (2008). A barrier nucleosome model for statistical positioning of nucleosomes
1044 throughout the yeast genome. *Genome Research*.
1045 <https://doi.org/10.1101/gr.078261.108>

1046 Mazur, D. J., Mendillo, M. L., & Kolodner, R. D. (2006). Inhibition of Msh6 ATPase
1047 Activity by Mismatched DNA Induces a Msh2(ATP)-Msh6(ATP) State Capable of
1048 Hydrolysis-Independent Movement along DNA. *Molecular Cell*.

1049 <https://doi.org/10.1016/j.molcel.2006.02.010>
 1050 McSwiggen, D., Hansen, A., Marie-Nelly, H., Teves, S., Heckert, A., Dugast-Darzacq,
 1051 C., ... Darzacq, X. (2018). Transient DNA Binding Induces RNA Polymerase II
 1052 Compartmentalization During Herpesviral Infection Distinct From Phase Separation.
 1053 *BioRxiv*. <https://doi.org/10.1101/375071>
 1054 Mehta, G. D., Ball, D. A., Eriksson, P. R., Chereji, R. V., Clark, D. J., McNally, J. G., &
 1055 Karpova, T. S. (2018). Single-Molecule Analysis Reveals Linked Cycles of RSC
 1056 Chromatin Remodeling and Ace1p Transcription Factor Binding in Yeast. *Molecular*
 1057 *Cell*. <https://doi.org/10.1016/j.molcel.2018.09.009>
 1058 Morillon, A., Karabetsov, N., O'Sullivan, J., Kent, N., Proudfoot, N., & Mellor, J. (2003).
 1059 Isw1 Chromatin Remodeling ATPase Coordinates Transcription Elongation and
 1060 Termination by RNA Polymerase II. *Cell*. [https://doi.org/10.1016/S0092-](https://doi.org/10.1016/S0092-8674(03)00880-8)
 1061 [8674\(03\)00880-8](https://doi.org/10.1016/S0092-8674(03)00880-8)
 1062 Morrison, A. J., Highland, J., Krogan, N. J., Arbel-Eden, A., Greenblatt, J. F., Haber, J.
 1063 E., & Shen, X. (2004). INO80 and γ -H2AX Interaction Links ATP-Dependent
 1064 Chromatin Remodeling to DNA Damage Repair. *Cell*, 119(6), 767–775.
 1065 <https://doi.org/10.1016/J.CELL.2004.11.037>
 1066 Neely, K. E., Hassan, A. H., Wallberg, A. E., Steger, D. J., Cairns, B. R., Wright, A. P.
 1067 H., & Workman, J. L. (1999). Activation domain-mediated targeting of the SWI/SNF
 1068 complex to promoters stimulates transcription from nucleosome arrays. *Molecular*
 1069 *Cell*. [https://doi.org/10.1016/S1097-2765\(00\)80216-6](https://doi.org/10.1016/S1097-2765(00)80216-6)
 1070 Neumann, F. R., Dion, V., Gehlen, L. R., Tsai-Pflugfelder, M., Schmid, R., Taddei, A., &
 1071 Gasser, S. M. (2012). Targeted INO80 enhances subnuclear chromatin movement
 1072 and ectopic homologous recombination. *Genes and Development*.
 1073 <https://doi.org/10.1101/gad.176156.111>
 1074 Nguyen, V. Q., Ranjan, A., Liu, S., Tang, X., Ling, Y. H., Wisniewski, J., ... Wu, C.
 1075 (2021). Spatio-Temporal Coordination of Transcription Preinitiation Complex
 1076 Assembly in Live Cells. *Molecular Cell*, *In press*, Sept 2, 2021 publication date.
 1077 Ocampo, J., Chereji, R. V., Eriksson, P. R., & Clark, D. J. (2016). The ISW1 and CHD1
 1078 ATP-dependent chromatin remodelers compete to set nucleosome spacing in vivo.
 1079 *Nucleic Acids Research*. <https://doi.org/10.1093/nar/gkw068>

- Ocampo, J., Chereji, R. V., Eriksson, P. R., & Clark, D. J. (2019). Contrasting roles of the RSC and ISW1/CHD1 chromatin remodelers in RNA polymerase II elongation and termination. *Genome Research*. <https://doi.org/10.1101/gr.242032.118>
- Parnell, T. J., Schlichter, A., Wilson, B. G., & Cairns, B. R. (2015). The chromatin remodelers RSC and ISW1 display functional and chromatin-based promoter antagonism. *ELife*. <https://doi.org/10.7554/eLife.06073>
- Persson, F., Lindén, M., Unoson, C., & Elf, J. (2013). Extracting intracellular diffusive states and transition rates from single-molecule tracking data. *Nature Methods*. <https://doi.org/10.1038/nmeth.2367>
- Peterson, C. L., & Workman, J. L. (2000). Promoter targeting and chromatin remodeling by the SWI/SNF complex. *Current Opinion in Genetics and Development*. [https://doi.org/10.1016/S0959-437X\(00\)00068-X](https://doi.org/10.1016/S0959-437X(00)00068-X)
- Prajapati, H. K., Ocampo, J., & Clark, D. J. (2020). Interplay among atp-dependent chromatin remodelers determines chromatin organisation in yeast. *Biology*, 9(8), 1–23. <https://doi.org/10.3390/biology9080190>
- Qiu, Y., Levendosky, R., Chakravarthy, S., Patel, A., Myong, S., States, U., ... States, U. (2018). HHS Public Access, 68(1), 76–88. <https://doi.org/10.1016/j.molcel.2017.08.018>
- Radman-Livaja, M., Quan, T. K., Valenzuela, L., Armstrong, J. A., van Welsem, T., Kim, T. S., ... Hartzog, G. A. (2012). A key role for Chd1 in histone H3 dynamics at the 3' ends of long genes in yeast. *PLoS Genetics*. <https://doi.org/10.1371/journal.pgen.1002811>
- Ramachandran, S., Zentner, G. E., & Henikoff, S. (2015). Asymmetric nucleosomes flank promoters in the budding yeast genome. *Genome Research*, 25(3), 381–390. <https://doi.org/10.1101/gr.182618.114>
- Rando, O. J., & Winston, F. (2012). Chromatin and transcription in yeast. *Genetics*. <https://doi.org/10.1534/genetics.111.132266>
- Ranjan, A., Nguyen, V. Q., Liu, S., Wisniewski, J., Kim, J. M., Tang, X., ... Wu, C. (2020). Live-cell single particle imaging reveals the role of RNA polymerase II in histone H2A.Z eviction. *ELife*. <https://doi.org/10.7554/elife.55667>
- Rossi, M. J., Kuntala, P. K., Lai, W. K. M., Yamada, N., Badjatia, N., Mittal, C., ... Pugh,

1111 B. F. (2021). A high-resolution protein architecture of the budding yeast genome.
 1112 *Nature*. <https://doi.org/10.1038/s41586-021-03314-8>

1113 Rothstein, R. (1991). Targeting, Disruption, Replacement, and Allele Rescue:
 1114 Integrative DNA Transformation in Yeast. *Methods in Enzymology*.
 1115 [https://doi.org/10.1016/0076-6879\(91\)94022-5](https://doi.org/10.1016/0076-6879(91)94022-5)

1116 Rust, M. J., Bates, M., & Zhuang, X. (2006). Stochastic optical reconstruction
 1117 microscopy (STORM) provides sub-diffraction-limit image resolution. *Nature*
 1118 *Methods*, 3(10), 793. <https://doi.org/10.1038/NMETH929>

1119 Ryan, D. P., Sundaramoorthy, R., Martin, D., Singh, V., & Owen-Hughes, T. (2011). The
 1120 DNA-binding domain of the Chd1 chromatin-remodelling enzyme contains SANT
 1121 and SLIDE domains. *EMBO Journal*, 30(13), 2596–2609.
 1122 <https://doi.org/10.1038/emboj.2011.166>

1123 Sabantsev, A., Levendosky, R. F., Zhuang, X., Bowman, G. D., & Deindl, S. (2019).
 1124 Direct observation of coordinated DNA movements on the nucleosome during
 1125 chromatin remodelling. *Nature Communications*, 10(1), 1–12.
 1126 <https://doi.org/10.1038/s41467-019-09657-1>

1127 Saha, A., Wittmeyer, J., & Cairns, B. R. (2005). Chromatin remodeling through
 1128 directional DNA translocation from an internal nucleosomal site. *Nature Structural*
 1129 *and Molecular Biology*, 12(9), 747–755. <https://doi.org/10.1038/nsmb973>

1130 Schick, S., Grosche, S., Kohl, K. E., Drpic, D., Jaeger, M. G., Marella, N. C., ... Kubicek,
 1131 S. (2021). Acute BAF perturbation causes immediate changes in chromatin
 1132 accessibility. *Nature Genetics*. <https://doi.org/10.1038/s41588-021-00777-3>

1133 Shimada, K., Oma, Y., Schleker, T., Kugou, K., Ohta, K., Harata, M., & Gasser, S. M.
 1134 (2008). Ino80 Chromatin Remodeling Complex Promotes Recovery of Stalled
 1135 Replication Forks. *Current Biology*. <https://doi.org/10.1016/j.cub.2008.03.049>

1136 Singleton, M. R., Dillingham, M. S., & Wigley, D. B. (2007). Structure and Mechanism of
 1137 Helicases and Nucleic Acid Translocases. *Annual Review of Biochemistry*, 76(1),
 1138 23–50. <https://doi.org/10.1146/annurev.biochem.76.052305.115300>

1139 Sirinakis, G., Clapier, C. R., Gao, Y., Viswanathan, R., Cairns, B. R., & Zhang, Y. (2011).
 1140 The RSC chromatin remodelling ATPase translocates DNA with high force and
 1141 small step size. *EMBO Journal*, 30(12), 2364–2372.

1142 <https://doi.org/10.1038/emboj.2011.141>

1143 Smolle, M., Venkatesh, S., Gogol, M. M., Li, H., Zhang, Y., Florens, L., ... Workman, J.
 1144 L. (2012a). Chromatin remodelers Isw1 and Chd1 maintain chromatin structure
 1145 during transcription by preventing histone exchange. *Nature Structural and*
 1146 *Molecular Biology*. <https://doi.org/10.1038/nsmb.2312>

1147 Smolle, M., Venkatesh, S., Gogol, M. M., Li, H., Zhang, Y., Florens, L., ... Workman, J.
 1148 L. (2012b). Chromatin remodelers Isw1 and Chd1 maintain chromatin structure
 1149 during transcription by preventing histone exchange. *Nature Structural and*
 1150 *Molecular Biology*. <https://doi.org/10.1038/nsmb.2312>

1151 Soutoglou, E., & Misteli, T. (2007). Mobility and immobility of chromatin in transcription
 1152 and genome stability. *Current Opinion in Genetics and Development*.
 1153 <https://doi.org/10.1016/j.gde.2007.08.004>

1154 Spain, M. M., Ansari, S. A., Pathak, R., Palumbo, M. J., Morse, R. H., & Govind, C. K.
 1155 (2014). The RSC Complex Localizes to Coding Sequences to Regulate Pol II and
 1156 Histone Occupancy. *Molecular Cell*. <https://doi.org/10.1016/j.molcel.2014.10.002>

1157 Strom, A. R., Emelyanov, A. V., Mir, M., Fyodorov, D. V., Darzacq, X., & Karpen, G. H.
 1158 (2017). Phase separation drives heterochromatin domain formation. *Nature*.
 1159 <https://doi.org/10.1038/nature22989>

1160 Struhl, K., & Segal, E. (2013). Determinants of nucleosome positioning. *Nature*
 1161 *Structural and Molecular Biology*, 20(3), 267–273.
 1162 <https://doi.org/10.1038/nsmb.2506>

1163 Tatavosian, R., Duc, H. N., Huynh, T. N., Fang, D., Schmitt, B., Shi, X., ... Ren, X.
 1164 (2018). Live-cell single-molecule dynamics of PcG proteins imposed by the DIPG
 1165 H3.3K27M mutation. *Nature Communications*. [https://doi.org/10.1038/s41467-018-](https://doi.org/10.1038/s41467-018-04455-7)
 1166 [04455-7](https://doi.org/10.1038/s41467-018-04455-7)

1167 Thompson, R. E., Larson, D. R., & Webb, W. W. (2002). Precise nanometer localization
 1168 analysis for individual fluorescent probes. *Biophysical Journal*, 82(5), 2775–2783.
 1169 [https://doi.org/10.1016/S0006-3495\(02\)75618-X](https://doi.org/10.1016/S0006-3495(02)75618-X)

1170 Tóth, J., Bollins, J., & Szczelkun, M. D. (2015). Re-evaluating the kinetics of ATP
 1171 hydrolysis during initiation of DNA sliding by Type III restriction enzymes. *Nucleic*
 1172 *Acids Research*. <https://doi.org/10.1093/nar/gkv1154>

1173 Tran, H. G., Steger, D. J., Iyer, V. R., & Johnson, A. D. (2000). The chrome domain
 1174 protein Chd1p from budding yeast is an ATP-dependent chromatin-modifying factor.
 1175 *EMBO Journal*. <https://doi.org/10.1093/emboj/19.10.2323>
 1176 Tsukiyama, T., Palmer, J., Landel, C. C., Shiloach, J., & Wu, C. (1999).
 1177 Characterization of the imitation switch subfamily of ATP-dependent chromatin-
 1178 remodeling factors in *Saccharomyces cerevisiae*. *Genes and Development*.
 1179 <https://doi.org/10.1101/gad.13.6.686>
 1180 Vallotton, P., & Olivier, S. (2013). Tri-track: Free software for large-scale particle
 1181 tracking. *Microscopy and Microanalysis*.
 1182 <https://doi.org/10.1017/S1431927612014328>
 1183 Van Attikum, H., Fritsch, O., Hohn, B., & Gasser, S. M. (2004). Recruitment of the
 1184 INO80 Complex by H2A Phosphorylation Links ATP-Dependent Chromatin
 1185 Remodeling with DNA Double-Strand Break Repair. *Cell*, 119(6), 777–788.
 1186 <https://doi.org/10.1016/J.CELL.2004.11.033>
 1187 Vary, J. C., Gangaraju, V. K., Qin, J., Landel, C. C., Kooperberg, C., Bartholomew, B., &
 1188 Tsukiyama, T. (2003). Yeast Isw1p forms two separable complexes in vivo.
 1189 *Molecular and Cellular Biology*. <https://doi.org/10.1128/MCB.23.1.80-91.2003>
 1190 Vincent, J. A., Kwong, T. J., & Tsukiyama, T. (2008). ATP-dependent chromatin
 1191 remodeling shapes the DNA replication landscape. *Nature Structural and Molecular*
 1192 *Biology*, 15(5), 477–484. <https://doi.org/10.1038/nsmb.1419>
 1193 Von Hippel, P. H., & Berg, O. G. (1989). Facilitated target location in biological systems.
 1194 *Journal of Biological Chemistry*.
 1195 Wagner, F. R., Dienemann, C., Wang, H., Stützer, A., Tegunov, D., Urlaub, H., &
 1196 Cramer, P. (2020). Structure of SWI/SNF chromatin remodeller RSC bound to a
 1197 nucleosome. *Nature*. <https://doi.org/10.1038/s41586-020-2088-0>
 1198 Walker, J. E., Saraste, M., Runswick, M. J., & Gay, N. J. (1982). Distantly related
 1199 sequences in the alpha- and beta-subunits of ATP synthase, myosin, kinases and
 1200 other ATP-requiring enzymes and a common nucleotide binding fold. *The EMBO*
 1201 *Journal*. <https://doi.org/10.1002/j.1460-2075.1982.tb01276.x>
 1202 Whitehouse, I., Rando, O. J., Delrow, J., & Tsukiyama, T. (2007). Chromatin
 1203 remodelling at promoters suppresses antisense transcription. *Nature*, 450(7172),

1204 1031–1035. <https://doi.org/10.1038/nature06391>

1205 Whitehouse, I., Stockdale, C., Flaus, A., Szczelkun, M. D., & Owen-Hughes, T. (2003).
 1206 Evidence for DNA Translocation by the ISWI Chromatin-Remodeling Enzyme.
 1207 *Molecular and Cellular Biology*. <https://doi.org/10.1128/mcb.23.6.1935-1945.2003>

1208 Wu, C. (1980). The 5' ends of drosophila heat shock genes in chromatin are
 1209 hypersensitive to DNase I. *Nature*. <https://doi.org/10.1038/286854a0>

1210 Yen, K., Vinayachandran, V., Batta, K., Koerber, R. T., & Pugh, B. F. (2012). Genome-
 1211 wide nucleosome specificity and directionality of chromatin remodelers. *Cell*.
 1212 <https://doi.org/10.1016/j.cell.2012.04.036>

1213 Yildiz, A., Forkey, J. N., McKinney, S. A., Ha, T., Goldman, Y. E., & Selvin, P. R. (2003).
 1214 Myosin V Walks Hand-Over-Hand: Single Fluorophore Imaging with 1.5-nm
 1215 Localization. *Science*, 300(5628), 2061 LP – 2065.
 1216 <https://doi.org/10.1126/science.1084398>

1217 Yuan, G.-C., Liu, Y.-J., Dion, M. F., Slack, M. D., Wu, L. F., Altschuler, S. J., & Rando,
 1218 O. J. (2005). Genome-scale identification of nucleosome positions in
 1219 *Saccharomyces cerevisiae*. *Nature Methods*. [https://doi.org/10.1038/nmeth0805-](https://doi.org/10.1038/nmeth0805-567)
 1220 567

1221 Yudkovsky, N., Logie, C., Hahn, S., & Peterson, C. L. (1999). Recruitment of the
 1222 SWI/SNF chromatin remodeling complex by transcriptional activators. *Genes and*
 1223 *Development*. <https://doi.org/10.1101/gad.13.18.2369>

1224 Zentner, G. E., Tsukiyama, T., & Henikoff, S. (2013). ISWI and CHD Chromatin
 1225 Remodelers Bind Promoters but Act in Gene Bodies. *PLoS Genetics*, 9(2),
 1226 e1003317. <https://doi.org/10.1371/journal.pgen.1003317>

1227 Zhang, Z., Wippo, C. J., Wal, M., Ward, E., Korber, P., & Pugh, B. F. (2011). A packing
 1228 mechanism for nucleosome organization reconstituted across a eukaryotic genome.
 1229 *Science*. <https://doi.org/10.1126/science.1200508>

1230 Zheng, Q., Ayala, A. X., Chung, I., Weigel, A. V., Ranjan, A., Falco, N., ... Lavis, L. D.
 1231 (2019a). Rational Design of Fluorogenic and Spontaneously Blinking Labels for
 1232 Super-Resolution Imaging. *ACS Central Science*.
 1233 <https://doi.org/10.1021/acscentsci.9b00676>

1234 Zheng, Q., Ayala, A. X., Chung, I., Weigel, A. V., Ranjan, A., Falco, N., ... Lavis, L. D.

(2019b). Rational Design of Fluorogenic and Spontaneously Blinking Labels for Super-Resolution Imaging. <https://doi.org/10.1021/acscentsci.9b00676>

FIGURE LEGENDS

Figure 1. Chromatin-binding and chromatin-free fractions of RSC, SWI/SNF, INO80, and ISW2. **(A)** Experimental scheme. **(B)** Fast-tracking imaging regime uses short exposures (10 ms) at high laser power to distinguish slow (chromatin-bound) and fast (chromatin-free) diffusing populations. **(C)** Slow-tracking regime directly observes the dwell times of chromatin-bound molecules using 250 ms exposures at low laser power. **(D-G)** (Top) Raw displacement histograms over the first 5 time frames (Δt : 10, 20, 30, 40, 50 ms). A two-state kinetic model was used for fitting the CDF [black lines] in Spot-On. (Bottom) Spot-On kinetic modeling results based on displacement distribution histograms for Sth1-Halo **(D)**, Snf2-Halo **(E)**, Ino80-Halo **(F)**, and Isw2-Halo **(G)**. Solid colored bar with indicated value represents % chromatin-bound molecules; open bar represents % chromatin-free. Error bars are standard deviations from 2 [or 3 for ISW2] biological replicates.

Figure supplement 1. Cell growth, integrity, and localization of HaloTagged remodeler subunits.

Figure supplement 2. Spot-On kinetic modeling analysis.

Figure supplement 3. Yeast culture during imaging and laser illumination do not have obvious effects on remodeler diffusion.

Figure supplement 4. Log₁₀D histograms for six remodelers and Gaussian fitting.

Source data 1. MSD-based kinetic analysis.

Source data 2. Original gel images for Figure supplement 1A.

Figure 2. Chromatin-binding and chromatin-free populations of CHD1 and ISW1. **(A-B)** Spot-On analysis as described in Figure 1 for the catalytic subunits Chd1-Halo **(A)** and Isw1-Halo **(B)**. **(C-D)** Spot-On analysis of the accessory subunits of ISW1a and ISW1b complexes: loc3-Halo **(C)** and loc4-Halo **(D)**.

Figure 3. Remodelers undergo frequent transitions between bound and free states. **(A)** Halo-H2B (brown) and Halo-NLS (pink) molecules display well-separated peaks in their diffusion coefficient histograms. **(B)** An overview of displacement-based HMM classification (vbSPT) to identify transitioning trajectories. After classifying each displacement as either in bound or free state, each trajectory is sub-classified as 'bound only', 'free only', or 'transitioning'. **(C-I)** Left: Overlay of raw histograms of \log_{10} diffusion coefficients for 'Bsound only' (turquoise), 'Free only' (yellow), 'Transitioning' (purple), and total trajectories (thin black). Right: Quantification (%) of transitioning trajectories in the diffusion coefficient histogram, where errors represent standard deviation between 2 [or 3 for ISW2] biological replicates. **(C)** Transitioning trajectories for Halo-H2B (top) and Halo-NLS (bottom). **(D-I)** Transitioning trajectories for remodelers: Sth1-Halo (**D**), Snf2-Halo (**E**), Ino80-Halo (**F**), and Isw2-Halo (**G**), Chd1-Halo (**H**), and Isw1-Halo (**I**).

Figure supplement 1. Validation of two diffusive states classified by vbSPT, and quantification of transitioning frequencies.

Source data 1. vbSPT analysis.

Figure 4. All remodelers have short-lived stable-binding residence times of 4-7 s. **(A-F)** Fitted double exponential decay curves from 1-CDF plots of observed dwell times from individual binding events (n) imaged by slow-tracking, for Sth1-Halo (**A**) Snf2-Halo (**B**), Ino80-Halo (**C**), and Isw2-Halo (**D**), Chd1-Halo (**E**), and Isw1-Halo (**F**). Solid colored and dashed black fitted curves for indicated remodelers and H2B, respectively. Pie charts show the percentage (f_{sb}) and average residence time (τ_{sb}) of the stable binding population after photobleaching correction. Errors represent bootstrap resampling errors after resampling 100 times (sb: stable-binding; tb: transient-binding).

Figure supplement 1. Survival plots [1-CDF] of dwell times showing 1- vs 2-component exponential decay fits.

Source data 1. Kinetic parameters determined by slow-tracking.

Figure 5. ATP hydrolysis is responsible for rapid chromatin dissociation. **(A)** Bar diagram and cartoons for remodelers mutated in the 'Walker A' and 'Walker B' motifs, respectively. **(B)** Representative 3D plots of trajectories imaged by slow-tracking for

wildtype (Chd1-Halo, black) and ATPase-dead mutant (Chd1K407R-Halo, red). Each plot shows all trajectories (≥ 3 frames) from single nucleus where lines represent apparent durations of chromatin-binding events. **(C-F)** 1-CDF plot, pie chart, and residence times of wildtype (top) and ATPase-dead mutants (bottom) for Isw2 **(C)**, Isw1 **(D)**, and Chd1 **(E,F)**.

Figure supplement 1. Expression levels and 1-CDF plots for wildtype and mutant ATPase-dead Isw2D312N.

Source data 1. Slow-tracking for ATPase-dead mutants.

Source data 2. Original gel images for Figure supplement 1A.

Figure 6. ATP utilization is responsible for enhanced mobility of chromatin-bound remodeler. (A-B) Average MSD plot **(A)** and violin plot **(B)**, of individual D values for 'bound only' trajectories imaged by fast-tracking, shown for six remodelers and H2B histone. **(C)** Violin plot showing distribution of individual D values imaged by slow-tracking for six remodelers and H2B histone. For **(A-C)** each wildtype remodeler is compared to H2B by the ordinary one-way ANOVA test (**** $p < 0.0001$, *** $p < 0.001$, ** $p < 0.01$, * $p < 0.05$). **(D-H)** MSD plot **(D-F)** and violin plot **(G,H)** of individual D values for 'trajectories imaged by slow-tracking for wildtype, ATPase-dead mutant, and H2B. For violin plots, thick red and dotted gray lines represent the median and two quartiles, respectively. For **D-H**, mutants are compared to wildtype by the unpaired t test (**** $p < 0.0001$, *** $p < 0.001$, ns: not significant). **(I)** Representative trajectories imaged by slow-tracking for H2B and remodelers. H2B displays low mobility, whereas remodelers display higher chromatin-associated diffusivity that is enhanced by ATP utilization.

Figure supplement 1. Chromatin-bound remodelers display higher radius of confinement (R_c) values than H2B.

Source data 1. Number of molecules (N), statistical tests, and source data for Figure 6.

Figure 7. Remodelers show substantial temporal occupancies at chromatin targets. (A) Key parameters measured in this study and acquired from the literature (Ho et al., 2018; Kubik et al., 2019) are used to calculate occupancy levels for gene promoter-acting remodelers. **(B)** Time trace simulations of temporal occupancy for

individual remodelers at a target promoter region based on average τ_{sb} and sampling interval. Top and bottom bars represent occupied (on) and vacant (off) states, respectively, and vertical lines depict transitions between the two states. **(C)** Time trace simulations of occupancy at a RSC- and INO80-bound promoter region based on average τ_{sb} and sampling interval. Individual time trace simulations are shown above, and the cumulative simulated occupancy plot (black) shows either one or both remodelers bound in the time course of 500 s.

Figure supplement 1. Time trace simulations of temporal occupancies at promoters bound by multiple remodelers, and analysis of CHD1 DNA-binding mutant.

Figure 8. Nucleosome remodeling at promoters. Model for nucleosome remodeling cycle at a gene promoter region targeted by RSC, SWI/SNF, INO80, and ISW2. The promoter region transitions between remodeler-occupied [solid arrow] and remodeler-vacant [dashed arrow] states, and their mean durations are indicated. After association with the NDR, remodelers undergo 1-D diffusion on chromatin facilitated by ATP binding, resulting in higher chromatin-associated mobility. Upon engaging a nucleosome substrate [e.g. the +1 nucleosome], RSC or SWI/SNF uses the energy of ATP hydrolysis to ‘push’ the nucleosome away from the NDR and INO80 or ISW2 to ‘pull’ the nucleosome into the NDR. ATP hydrolysis facilitates remodeler dissociation, and the promoter region becomes vacant for other factor interactions. The order of remodeler visitation is arbitrary, and simultaneous co-occupancy within the NDR can occur (see text for details).

SUPPLEMENTAL INFORMATION

Figure 1-figure supplement 1. Cell growth, integrity, and localization of HaloTagged remodeler subunits.

(A) SDS-PAGE gel scanned for JF646 dye fluorescence (top) and imaged after Coomassie staining (bottom). Cell lysates are prepared by NaOH protein extraction method (Amberg et al., 2006) after treatment with JF646 at a saturating dye concentration (20 nM) for 2 h at 30°C. **(B)** JF646 dye fluorescence in the soluble supernatant (as shown in **A**) and insoluble pellet for Sth1-Halo strain. Substantial Sth1-

Halo protein is retained the insoluble pellet. **(C)** Overlay of Phase Contrast image and initial nuclear fluorescence captured by JF552 dye excitation of yeast stained with JF552. **(D)** Five-fold dilutions of HaloTag fusion and wildtype strains are plated on YPAD plates at the indicated temperatures for 2-3 days. **(E)** Relationship between D_{free} values determined by Spot-On analysis and the calculated molecular weights of chromatin remodeling complexes.

Figure 1-figure supplement 2. Spot-On kinetic modeling analysis.

(A) Kinetic parameters (F_{bound} , D_{bound} , D_{free}) determined by Spot-On analysis. Errors represent standard deviation between 2 [or 3 for ISW2] biological replicates.

Figure 1-figure supplement 3. Yeast culture during imaging and laser illumination do not have obvious effects on remodeler diffusion.

(A) Spot-On analyses were performed on movies acquired either in the ‘first half’ or ‘second half’ of an imaging session to compare the F_{bound} values between the two groups. **(B)** Spot-On analyses were performed on the ‘first half’ [1-2500 frames] and ‘second half’ [2501-5000 frames] of each movie ‘substack’ to compare the F_{bound} values between the two groups. Circles represent individual biological replicates with red lines indicating before-after changes for each replicate. Errors represent standard deviation between biological replicates. Comparison between ‘first half’ and ‘second half’ groups for each remodeler by ordinary one-way ANOVA test (ns: not significant).

Figure 1-figure supplement 4. Log₁₀D histograms for six remodelers and Gaussian fitting.

(A-H) Normalized histograms of log₁₀ diffusion coefficients of single-molecule trajectories fitted to two Gaussian distribution functions (solid gray line: sum of two Gaussians; dashed lines: individual Gaussian curves representing chromatin-bound and chromatin-free populations) for Sth1-Halo **(A)**, Snf2-Halo **(B)**, Ino80-Halo **(C)**, and Isw2-Halo **(D)**, Chd1-Halo **(E)**, and Isw1-Halo **(F)**, Ioc3-Halo **(G)**, and Ioc4-Halo **(H)**. The two components are not well-resolved.

Figure 3-figure supplement 1. Validation of two diffusive states classified by vbSPT, and quantification of transitioning frequencies.

(A) Pipeline for classification and sub-classification of trajectories using vbSPT. Individual displacement lengths were determined for ‘bound only’, ‘free only’, and ‘transitioning’-subclassified trajectories to validate the two states and state transitions. **(B-C)** Violin plot **(B)** and median value **(C)** of individual displacement lengths for the Bound and Free states in non-transitioning and transitioning trajectories. For violin plots, thick red and dotted gray lines represent the median and two quartiles, respectively. **(D-E)** Transitioning trajectories for loc3-Halo **(D)** and loc4-Halo **(E)**. Left: Overlay of raw histograms of \log_{10} diffusion coefficients for ‘Bound only’ (turquoise), ‘Free only’ (yellow), ‘Transitioning’ (purple), and total trajectories (thin black). Right: Quantification (%) of transitioning trajectories in the diffusion coefficient histogram. **(F)** For all classified transitioning trajectories, ‘FREE’ to ‘BOUND’ and ‘BOUND’ to ‘FREE’ transition frequencies are indicated. For **D-F**, errors represent standard deviation between 2 [or 3 for ISW2] biological replicates.

Figure 4-figure supplement 1. Survival plots [1-CDF] of dwell times showing 1- vs 2-component exponential decay fits.

(A-F) 1- and 2-component exponential decay fits to survival plots of dwell times for Sth1-Halo **(A)**, Snf2-Halo **(B)**, Ino80-Halo **(C)**, and Isw2-Halo **(D)**, Chd1-Halo **(E)**, and Isw1-Halo **(F)**. **(G)** 1-CDF plot, pie chart as in Figure 4, and residence times of loc3-Halo (Left) and loc4-Halo (Right). **(H)** 1- and 2-component exponential decay fits to survival plots of dwell times for loc3-Halo (Left) and loc4-Halo (Right).

Figure 5-figure supplement 1. Expression levels and 1-CDF plots for wildtype and mutant ATPase-dead Isw2D312N.

(A) SDS-PAGE analysis; gel scanned for JF646 dye fluorescence (top) and imaged after Coomassie staining (bottom). Cell lysates of ATPase mutants (Isw1K227R-Halo, Isw2K215R-Halo and Chd1D513N-Halo) and their wildtype strains were prepared after treatment with JF646 at a saturating dye concentration (20 nM) for 2 h at 30°C. **(B-E)** 1-CDF plot in log-log scale for Isw2K215R **(B)**, Isw1K227R **(C)**, Chd1K407R **(D)**, and

Chd1D513N (**E**) compared to wildtype. Colored dashed lines represent 95% confidence interval.

Figure 6-figure supplement 1. Chromatin-bound remodelers display higher radius of confinement (R_c) values than H2B.

(A) Radius of confinement values of bound trajectories in 10-ms exposure movies for histone H2B and chromatin remodelers. Violin plot showing distribution of R_c values, and comparison between histone H2B and each of wildtype remodelers by ordinary one-way ANOVA test. **(B)** Violin plot of individual D values by slow-tracking for Isw1-Halo after 30 min pre-treatment with 3 or 5 $\mu\text{g/mL}$ thiolutin, and comparison between wildtype and thiolutin-treated samples by unpaired t test (ns: not significant). Thick red and dotted gray lines represent the median and two quartiles, respectively.

Figure 7-figure supplement 1. Time trace simulations of temporal occupancies at promoters bound by multiple remodelers, and analysis of CHD1 DNA-binding mutant.

(A-B) Time trace simulations of occupancy as in Figure 6, at a promoter region bound by RSC, INO80, and ISW2 remodelers **(A)** or by RSC, SWI/SNF, INO80, and ISW2 remodelers **(B)**. Individual time trace simulations are shown above, and the cumulative simulated occupancy time trace (black) shows any one or multiple remodelers bound in the time course of 500 s. **(C-D)** Fast-tracking and slow-tracking results for CHD1 DNA-binding domain mutant (Chd1R1016A/K1020A/R1255A-Halo). (wildtype: dashed gray lines; DBD mutant: solid green lines). **(C)** Normalized histogram \log_{10} diffusion coefficients (Left) and Spot-On kinetic modeling results (Right). **(D)** 1-CDF plot, pie chart, and residence times.

Video 1. Fast-tracking movie (10 ms exposure/frame) for Sth1-Halo strain.

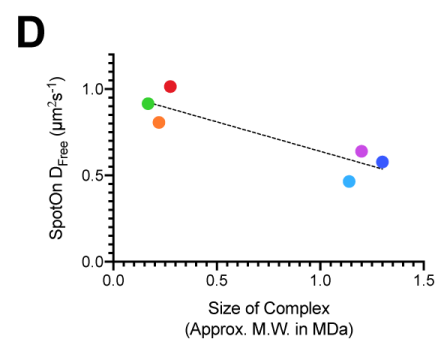
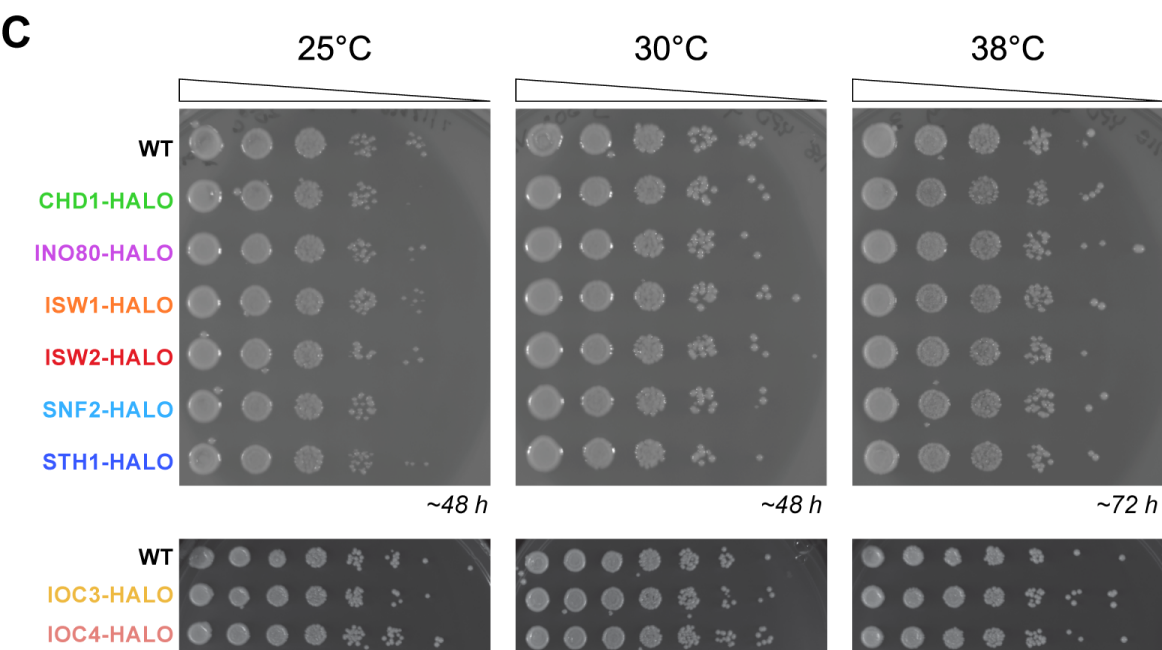
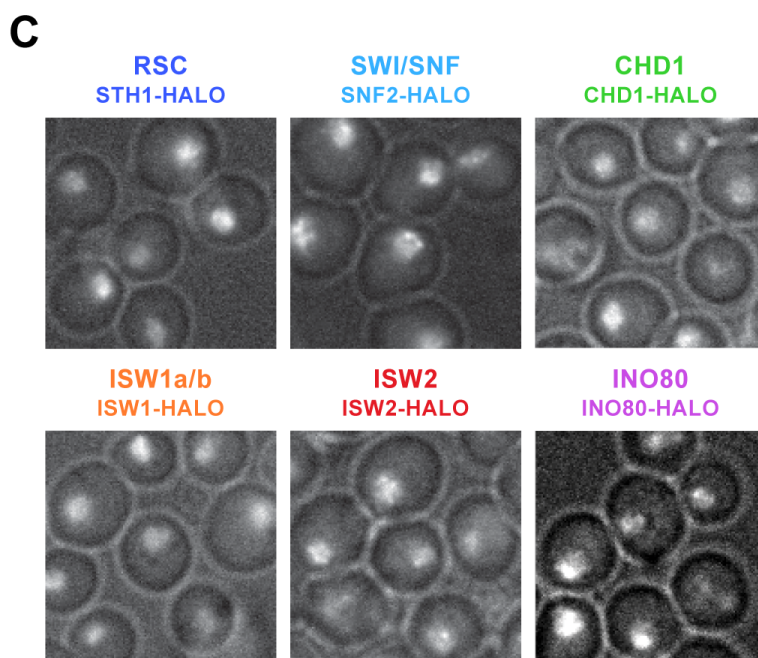
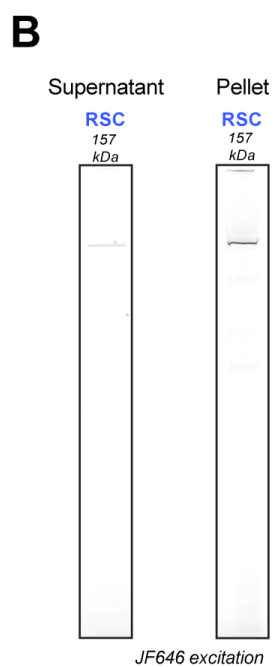
Related to Figure 1. Live-cell, single-molecule imaging of Sth1-Halo yeast cells stained with JF552. Movies with 10 ms exposure/frame were acquired with continuous 555 nm laser irradiation. Timestamp and scale bar (1 μm) are shown in the movie. White circles

1450 represent single nuclei. Last frame is an overlay of DIC image and initial nuclear
1451 fluorescence. Pixel: 107 nm.

1452

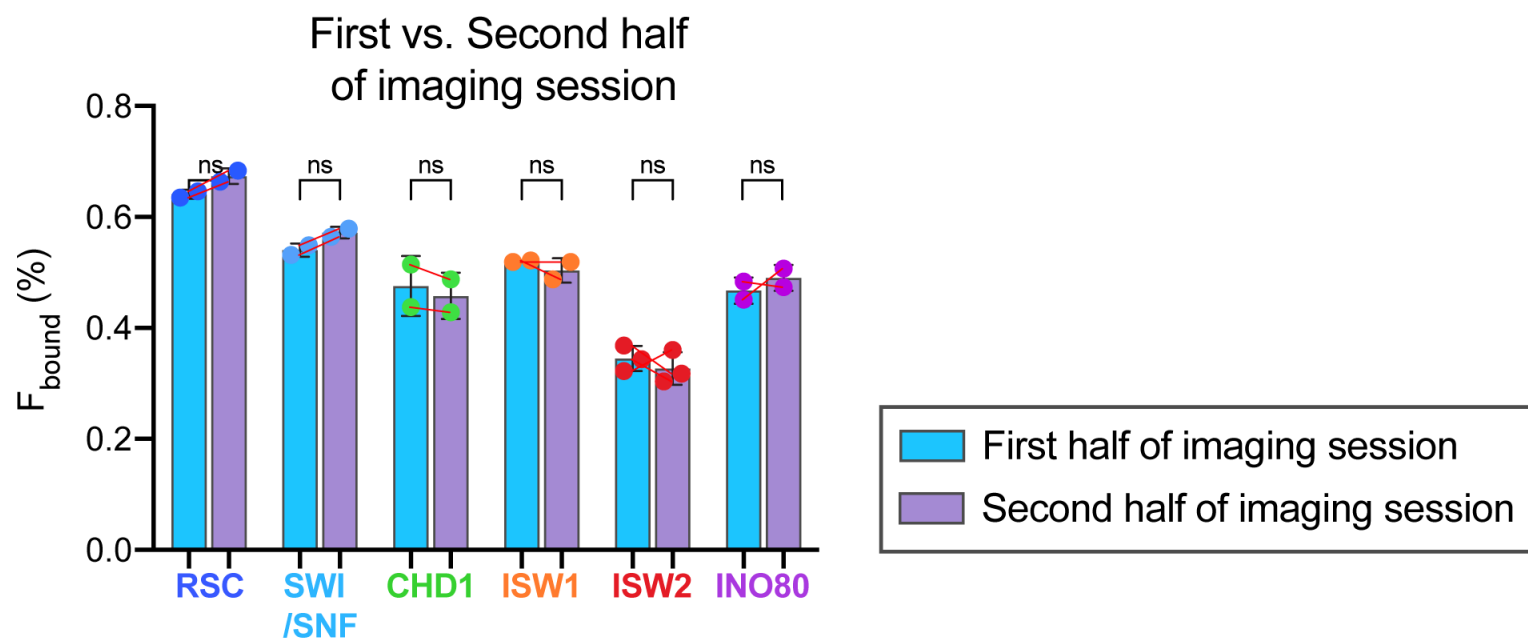
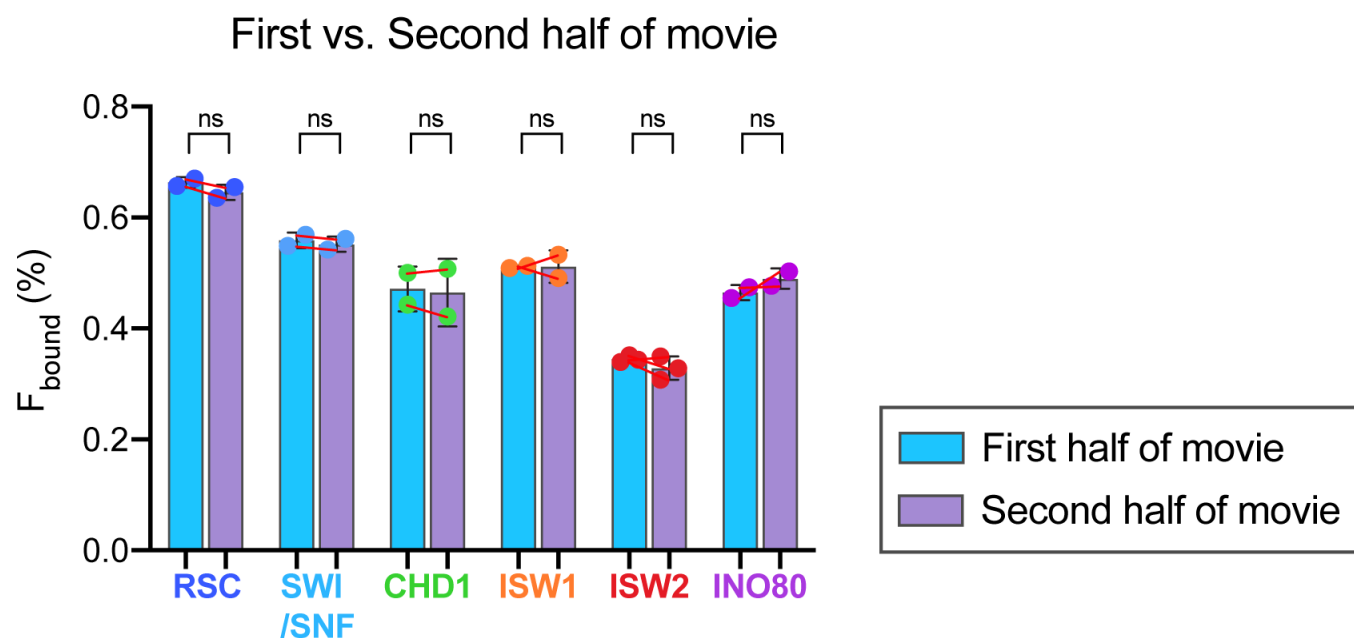
1453 **Supplementary file 1. List of Yeast strains used in this study**

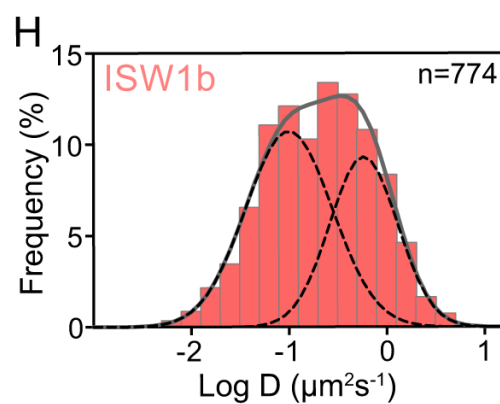
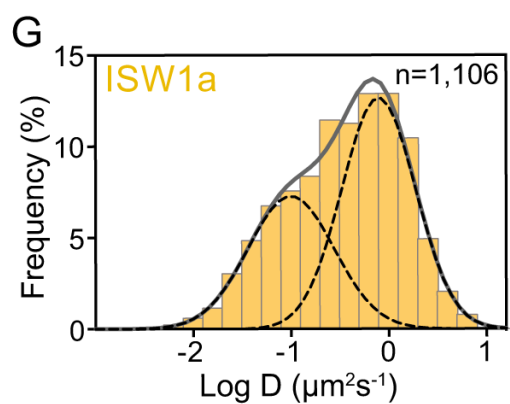
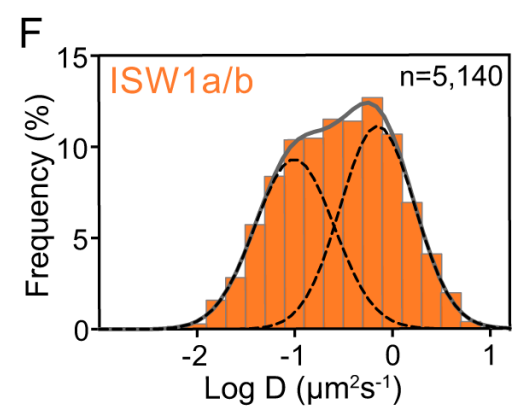
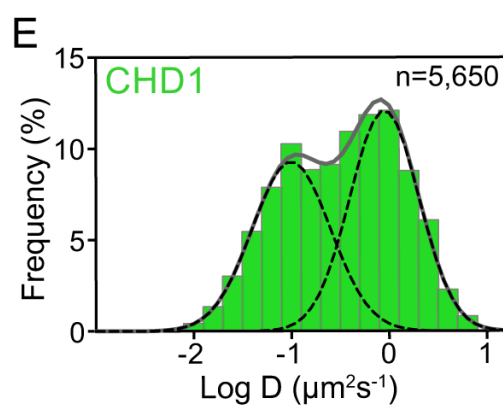
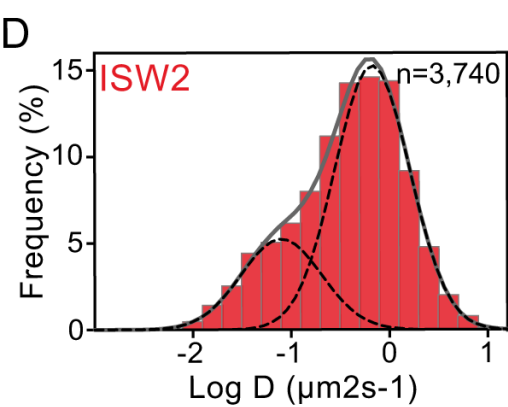
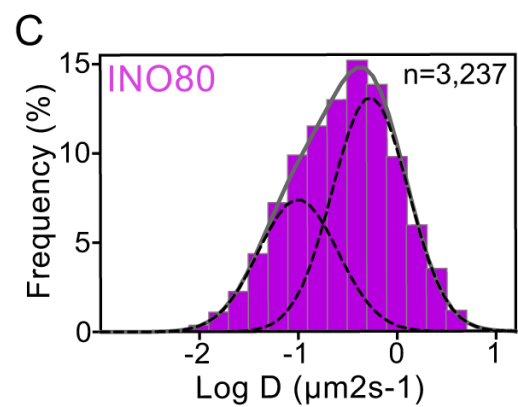
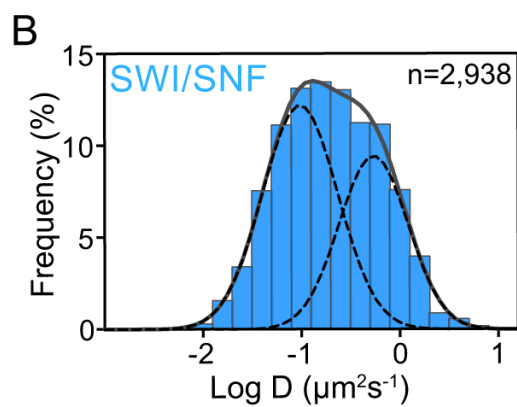
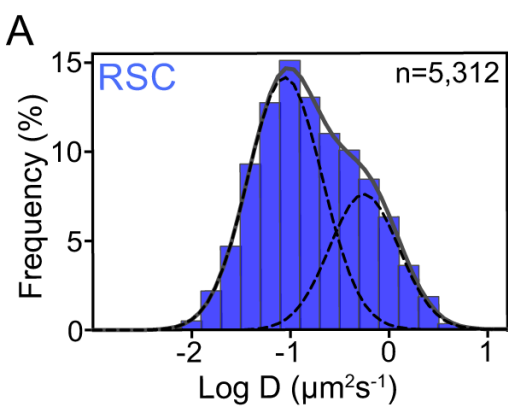
1454 **Supplementary file 2. List of oligonucleotides used in this study**

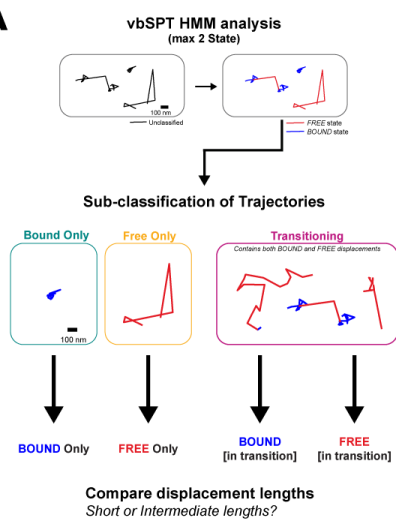
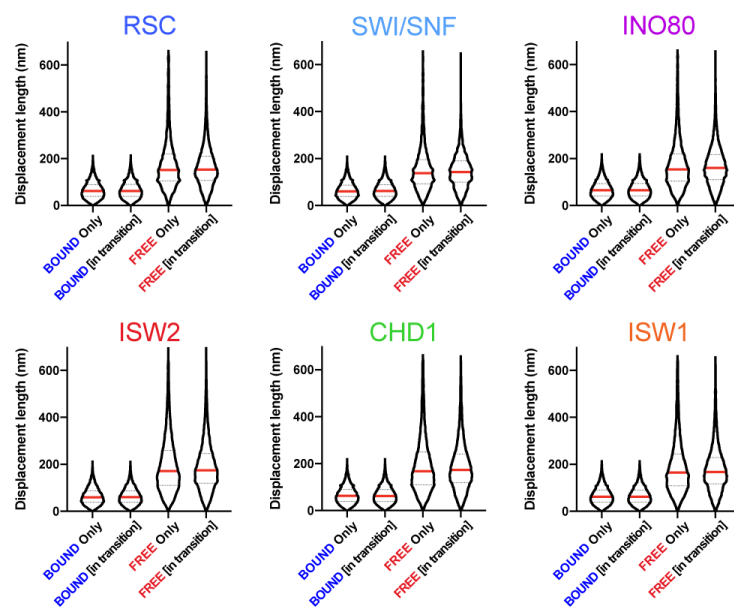
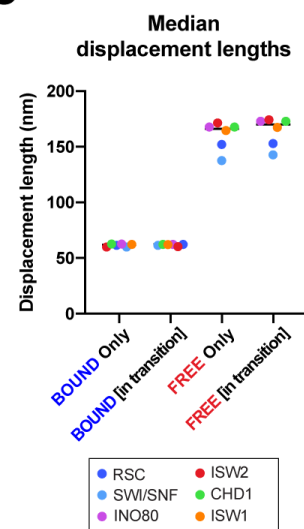
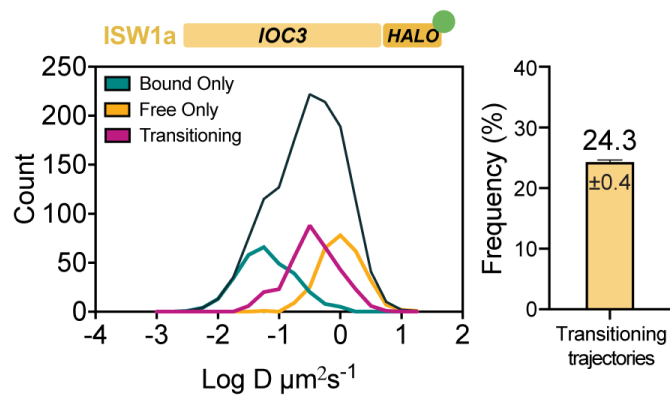
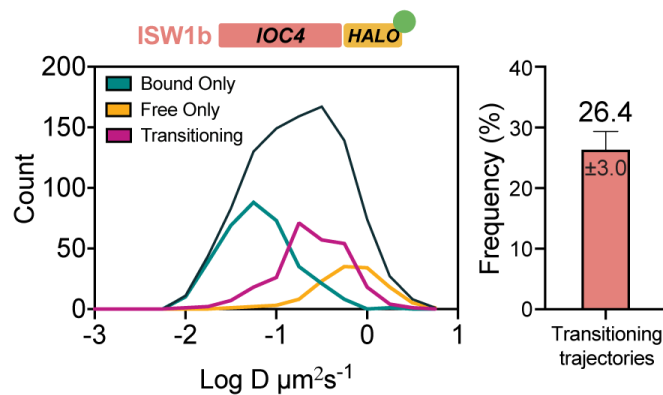
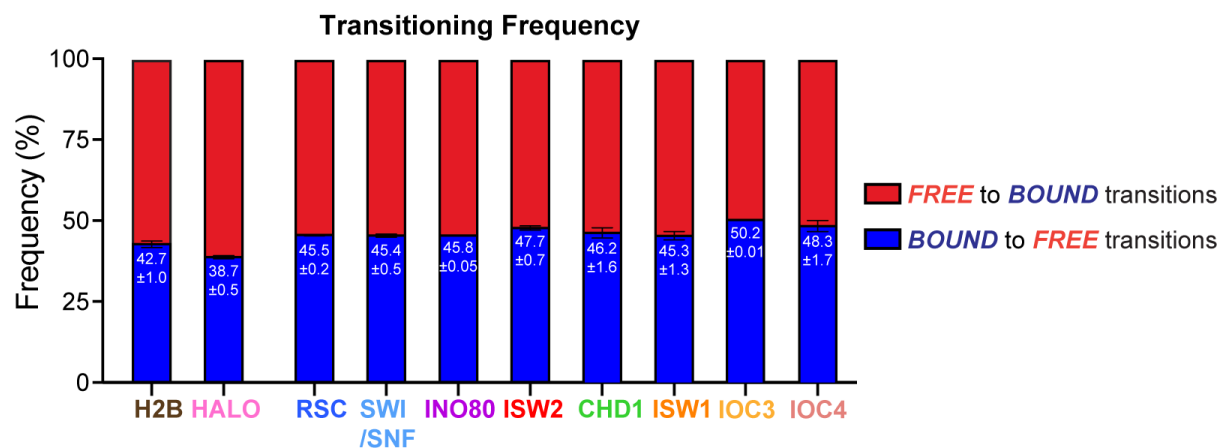


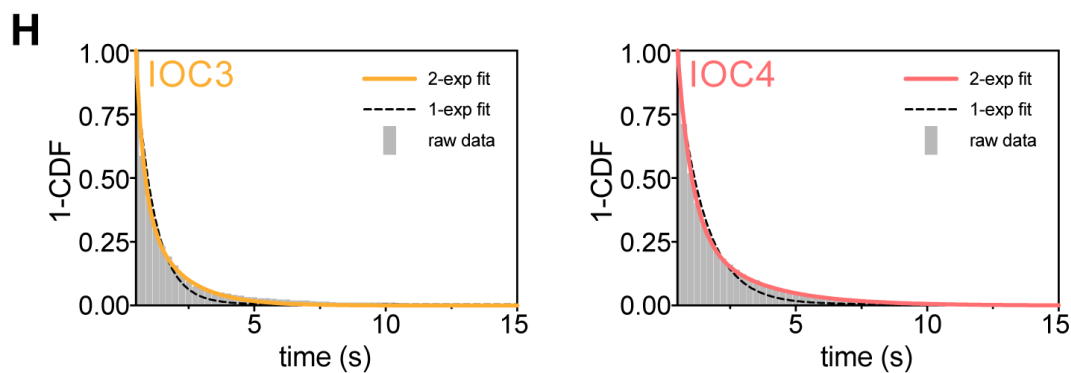
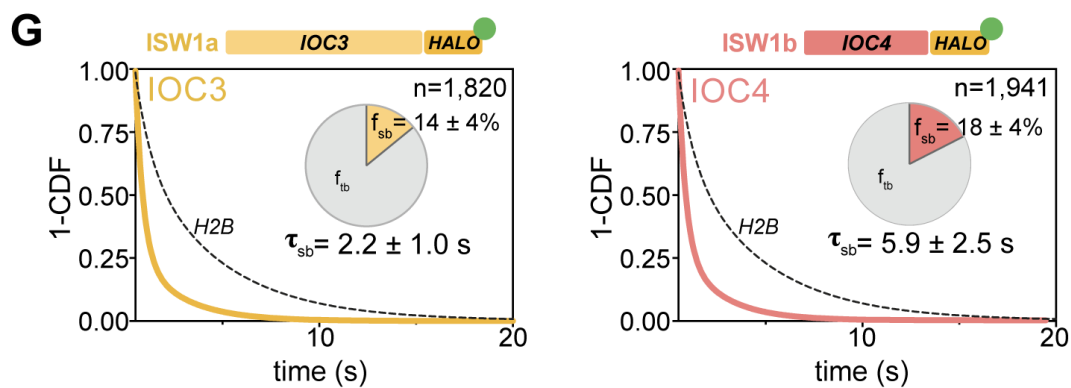
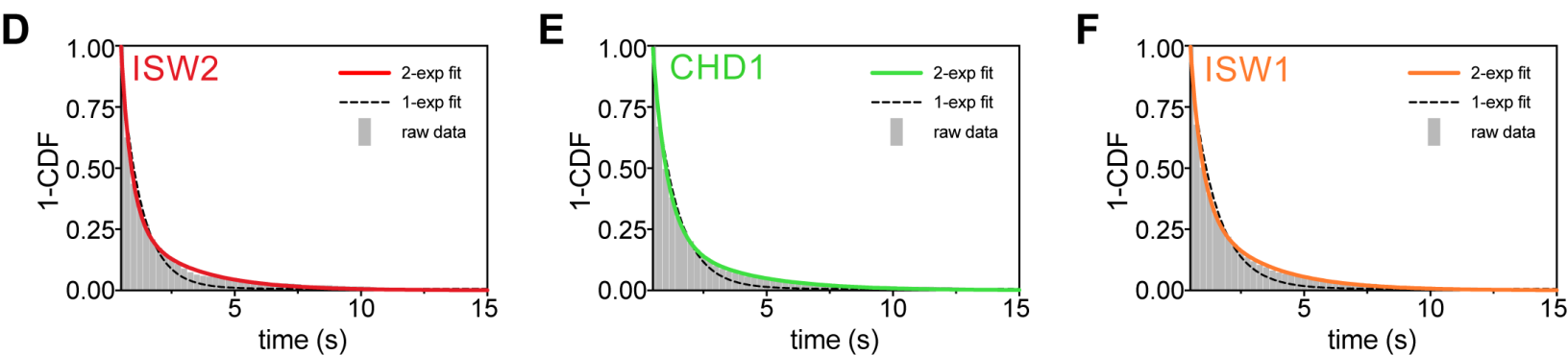
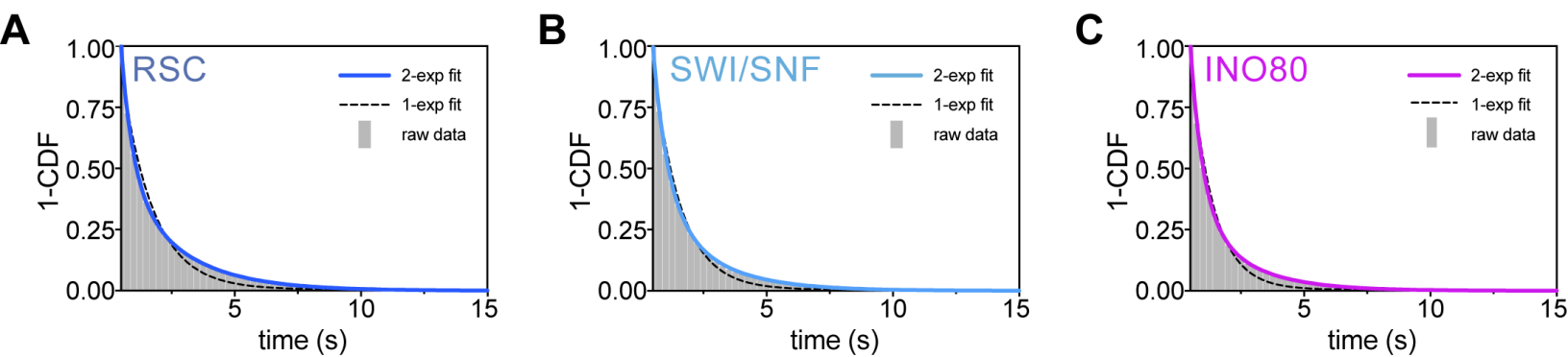
A

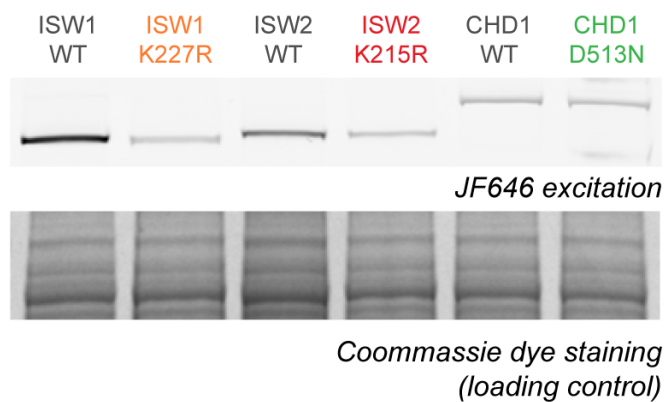
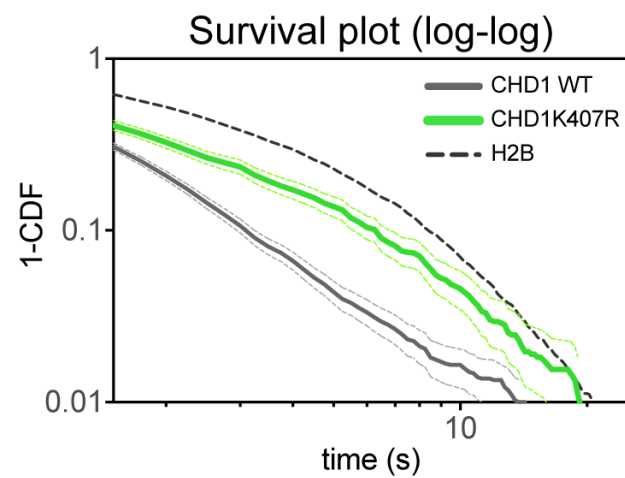
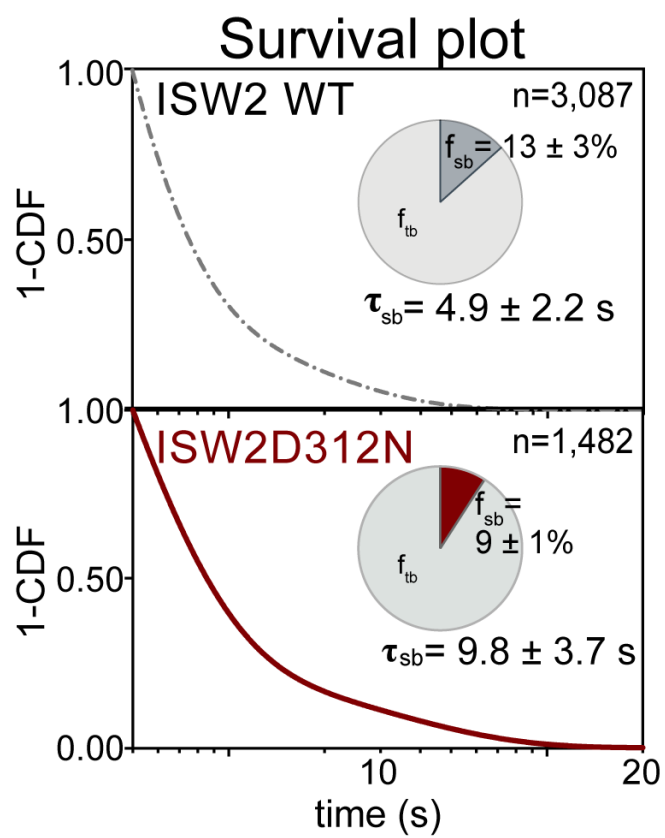
Remodeler	F_{bound} (%)	D_{bound} ($\mu\text{m}^2\text{s}^{-1}$)	D_{free} ($\mu\text{m}^2\text{s}^{-1}$)
RSC (Sth1)	66.0 ± 1.1	0.038 ± 0.002	0.577 ± 0.069
SWI/SNF (Snf2)	55.9 ± 1.3	0.036 ± 0.007	0.464 ± 0.043
INO80 (Ino80)	48.3 ± 0.2	0.050 ± 0.004	0.639 ± 0.058
ISW2 (Isw2)	34.8 ± 1.0	0.062 ± 0.001	1.014 ± 0.024
CHD1 (Chd1)	47.8 ± 4.9	0.047 ± 0.007	0.915 ± 0.038
ISW1a/b (Isw1)	52.0 ± 1.1	0.050 ± 0.001	0.806 ± 0.010
ISW1a (Ioc3)	39.6 ± 0.0	0.067 ± 0.004	0.791 ± 0.059
ISW1b (Ioc4)	55.5 ± 2.6	0.044 ± 0.005	0.532 ± 0.042
Histone H2B	79.4 ± 1.9	0.026 ± 0.000	0.970 ± 0.158

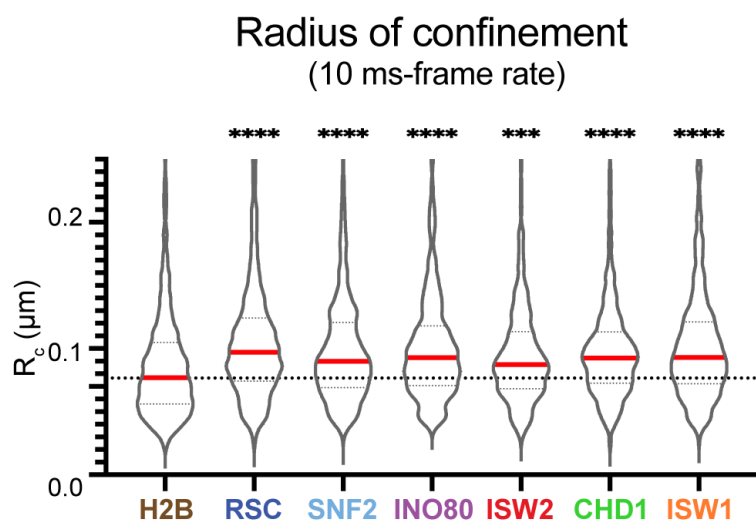
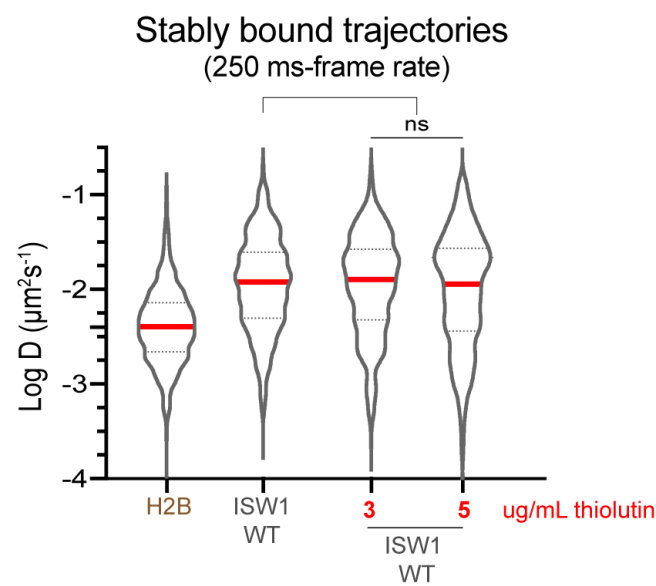
A**B**



A**B****C****D****E****F**

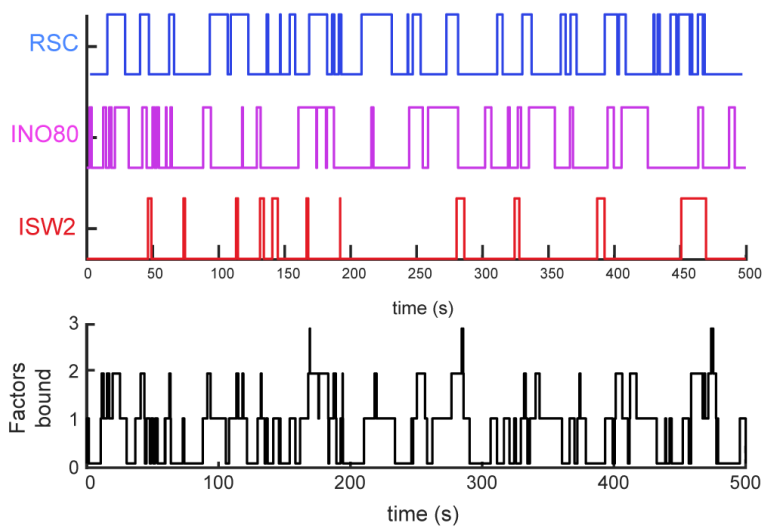


A**B****C**

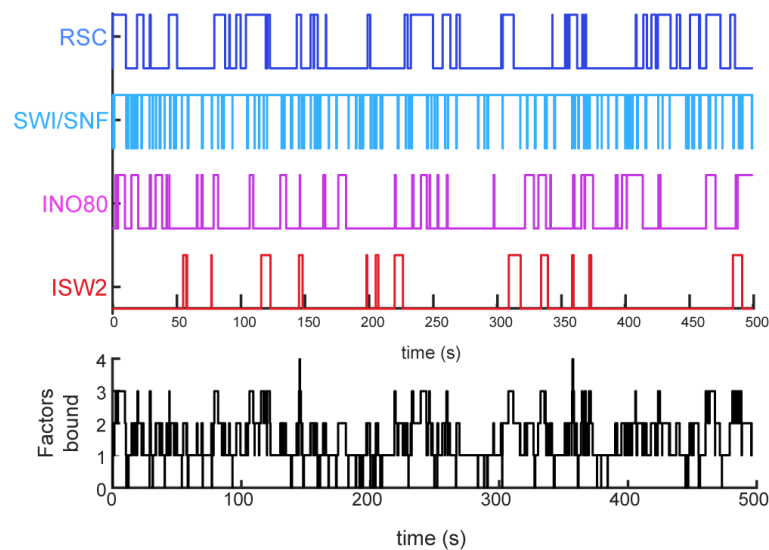
A**B**

A

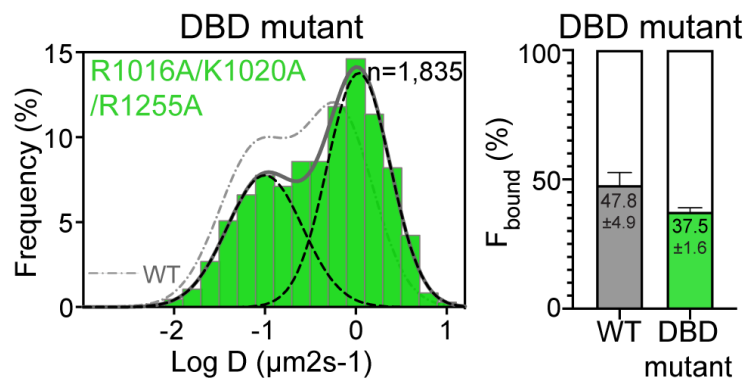
RSC, INO80, and ISW2-bound promoters

**B**

RSC, SWI/SNF, INO80, and ISW2-bound promoters

**C**

CHD1 CHD1 XXXX HALO

**D**